

Cross validation for penalized quantile regression with a case-weight adjusted solution path

Shanshan Tu* Yunzhang Zhu† Yoonkyung Lee‡ Qiuyu Gu§
Haozhen Yu¶

Abstract

Cross validation is widely used for selecting tuning parameters in regularization methods, but it is computationally intensive in general. To lessen its computational burden, approximation schemes such as generalized approximate cross validation (GACV) are often employed. However, such approximations may not work well when non-smooth loss functions are involved. As a case in point, approximate cross validation schemes for penalized quantile regression do not work well for extreme quantiles. In this paper, we propose a new algorithm to compute the leave-one-out cross validation scores exactly for quantile regression with ridge penalty through a case-weight adjusted solution path. Resorting to the homotopy technique in optimization, we introduce a case-weight for each individual data point as a continuous embedding parameter and decrease the weight gradually from one to zero to link the estimators based on the full data and those with a case deleted. This allows us to design a solution path algorithm to compute all leave-one-out estimators very efficiently from the full-data solution. We show that the case-weight adjusted solution path is piecewise linear in the weight parameter and using the solution path, we comprehensively examine case influences and observe that different modes of case influences emerge, depending on the specified quantiles, data dimensions and penalty parameter. We further illustrate the utility of the proposed algorithm in real-world applications.

Keywords: case influence, case-weight, cross validation, penalized M-estimation, solution path

1 Introduction

With the rapid growth of data dimensionality, regularization is widely used in model estimation and prediction. In penalized regression methods such as LASSO and ridge regression,

*Latitude AI, shanshantu23@gmail.com

†Amazon, ryzhux@gmail.com

‡Department of Statistics, The Ohio State University, yklee@stat.osu.edu

§Meta Platforms, Inc., qiuyugu15@gmail.com

¶Department of Statistics, The Ohio State University, yu.2823@osu.edu

the penalty parameter plays an essential role in determining the trade-off between bias and variance of the corresponding regression estimator. Too large a penalty could lead to undesirably large bias while too small a penalty would lead to instability in the estimator. The penalty parameter can be chosen to minimize the prediction error associated with the estimator. Cross validation (CV) (Stone, 1974) is the most commonly used technique for choosing the penalty parameter based on data-driven estimates of the prediction error, especially when there is not enough data available.

Typically, fold-wise CV is employed in practice. When the number of folds is the same as the sample size, it is known as leave-one-out (LOO) CV. For small data sets, LOO CV provides approximately unbiased estimates of the prediction error while the general k -fold CV may produce substantial bias due to the difference in sample size for the fold-wise training data and the original data (Kohavi, 1995). Moreover, for linear modeling procedures such as smoothing splines, the fitted values from the full data can be explicitly related to the predicted values for LOO CV (Craven and Wahba, 1979). Thus, the LOO CV scores are readily available from the full data fit. The linearity of a modeling procedure that enables exact LOO CV is strongly tied to squared error loss employed for the procedure and the simplicity of the corresponding optimality condition for the solution.

However, loss functions for general modeling procedures may not yield such simple optimality conditions as squared error loss does, and result in more complex relation between the fitted values and the observed responses. In general, the LOO predicted values may not be related to the full data fit in closed form. Consequently, the computation needed for LOO CV becomes generally intensive as LOO prediction has to be made for each of n cases separately given each candidate penalty parameter.

In this paper we focus on LOO CV for penalized M-estimation with nonsmooth loss functions, in particular, quantile regression with ridge penalty. Quantile regression (Koenker and Bassett, 1978) can provide a comprehensive description of the conditional distribution of the response variable given a set of covariates, and it has become an increasingly popular tool to explore the data heterogeneity (Koenker, 2017). Extreme quantiles can also

be used for outlier detection (Chaouch and Goga, 2010). Penalized quantile regression is particularly useful for analyzing high-dimensional heterogeneous data.

The check loss for quantile regression with a pre-specified quantile parameter $\tau \in (0, 1)$ is defined as

$$\rho_\tau(r) = \tau r_+ + (1 - \tau)(-r)_+, \text{ where } r_+ = \max(r, 0). \quad (1)$$

Unlike squared error loss, the check loss is nondifferentiable at 0 as is shown in Figure 1.

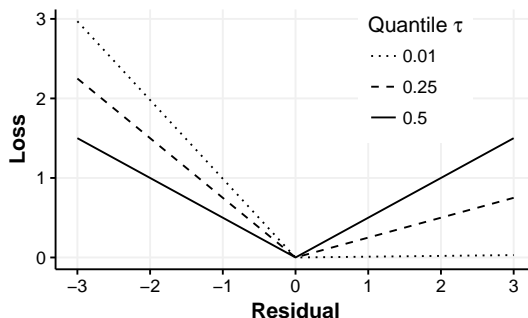


Figure 1: The check loss for quantile regression with quantile parameter $\tau = 0.01, 0.25$ and 0.5

To lessen the computational cost of the exact LOO CV in this setting, Nychka et al. (1995) and Yuan (2006) proposed Approximate CV (ACV) and Generalized Approximate CV (GACV). Using a smooth approximation of the check loss, they applied similar arguments used in mean regression for the derivation of ordinary cross validation (OCV) (Allen, 1971) and generalized cross validation (GCV) (Wahba et al., 1979) to quantile regression. The key ingredients for the arguments are the leave-one-out lemma and the first-order Taylor expansion of the smoothed check loss. The linearization error from the first-order Taylor expansion may not be ignorable for extreme quantiles due to the increasing skewness of the distribution of the LOO residuals that is at odds with the increase in the slope of the check loss with τ (see Section 4.1.1 for details). This phenomenon can be easily illustrated. Figure 2 compares the exact LOO CV and GACV scores as a function of the penalty parameter λ for various quantiles in a simulation setting (see Section 4 for details). For instance, the approximate CV scores in the figure could produce penalty parameter values that are

very different from the exact LOO CV when $\tau = 0.01$ and 0.1 . The empirical studies in [Li et al. \(2007\)](#) and [Reiss and Huang \(2012\)](#) also confirm the inaccuracy of the approximation for extreme quantiles. This result motivates us to explore other computationally efficient schemes for exact LOO CV.

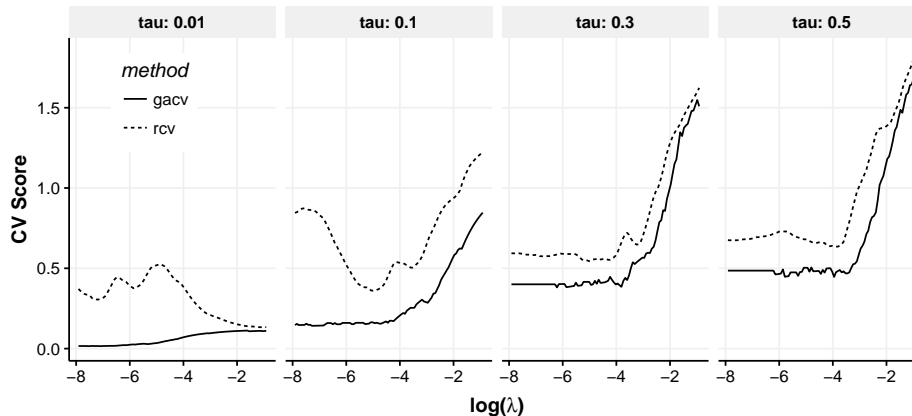


Figure 2: Comparison of the exact LOO CV and GACV scores for penalized quantile regression ($\tau = 0.01, 0.1, 0.3,$ and 0.5). The exact LOO CV score is defined as $RCV(\lambda) = \sum_{i=1}^n \rho_{\tau}(y_i - \hat{f}_{\lambda}^{[-i]}(x_i))/n$, and GACV score from [Li et al. \(2007\)](#) is defined as $GACV(\lambda) = \sum_{i=1}^n \rho_{\tau}(y_i - \hat{f}(x_i))/(n - |\mathcal{E}_{\lambda}|)$.

Instead of treating n LOO problems separately, we exploit the homotopy strategy to relate them to the full-data problem. The n LOO problems can be viewed as perturbations of the full-data problem. The key idea of homotopy is to start from a problem with known solution and gradually adjust the problem with respect to a continuous homotopy parameter until we reach the desired target problem and its solution. In our approach, we leverage the full-data solution as a starting point for the LOO problems. In optimization, homotopy techniques have been used in many algorithms including the interior point algorithm derived from perturbed KKT conditions ([Zhao et al., 2012](#)) and parametric active set programming ([Allgower and Georg, 1993](#)). In statistical learning community, the latter has been widely used in the form of path-following algorithms. For instance, [Osborne \(1992\)](#) and [Osborne et al. \(2000\)](#) apply the homotopy technique to generate piecewise linear trajectories in quantile regression and LASSO problems, respectively. Later [Efron et al. \(2004\)](#), [Hastie](#)

et al. (2004) and Rosset and Zhu (2007) exploit the homotopy path-following methods to generate an entire solution path for a family of regularization problems indexed by the penalty parameter.

In this paper, we propose an exact path-following algorithm for LOO cross validation in penalized quantile regression by introducing a case-weight ω for the held-out case as a continuous homotopy parameter. We vary the case-weight ω from 1 to 0 to link the full-data setting to the LOO setting. Let $\{(x_i, y_i)\}_{i=1}^n$ be the full data with covariates $x_i \in \mathbb{R}^p$ and response $y_i \in \mathbb{R}$. Given a fixed quantile τ and penalty parameter λ , for each case $i^* \in \{1, \dots, n\}$, consider the following case-weight adjusted quantile regression problem with linear regression quantiles:

$$\underset{\beta_0 \in \mathbb{R}, \beta \in \mathbb{R}^p}{\text{minimize}} \sum_{i \neq i^*} \rho_\tau(y_i - \beta_0 - x_i^\top \beta) + \omega \rho_\tau(y_{i^*} - \beta_0 - x_{i^*}^\top \beta) + \frac{\lambda}{2} \|\beta\|_2^2. \quad (2)$$

The problem in (2) with $\omega = 1$ involves the full data while $\omega = 0$ leaves out the case i^* . By decreasing the case-weight ω from 1 to 0, we successfully link the two separate but intrinsically related problems. Notice that the full data solution needs to be computed only once and can be used repeatedly as a starting point for n LOO problems. We provide an efficient homotopy algorithm to generate the solution path indexed by ω , which results in the LOO solution. Hence, with the LOO solutions, we can compute CV scores exactly, circumventing the issues with approximate CV especially for extreme quantiles.

There have been many works on computation of the solution paths for penalized quantile regression. In spirit of Hastie et al. (2004), Li and Zhu (2008) and Li et al. (2007) proposed algorithms for solution paths in λ given quantile τ in l_1 -penalized quantile regression and kernel quantile regression, respectively. By varying the quantile parameter τ , Takeuchi et al. (2009) examined the solution path as a function of τ for fixed λ in kernel quantile regression. Further, Rosset (2009) developed an algorithm for a generalized bi-level solution path as a function of both λ and τ . These algorithms are driven by a set of optimality conditions that imply piecewise linearity of the solution paths. Due to the linear structure

in the additional term with a case-weight ω in (2), it can be shown that the case-weight adjusted solution path is also piecewise linear in ω . This piecewise linearity allows us to devise a new path-following algorithm, which starts from the full-data solution and reaches the LOO solution at the end. We derive the optimality conditions for the case-weight adjusted solution and provide a formal proof that solutions from the algorithm satisfy the KKT conditions at every $\omega \in [0, 1]$.

The proposed path-following algorithm with a varying case-weight ω does not only offer the LOO solutions efficiently, but also provides case-influence measures. We demonstrate numerically and analytically that the computational cost of the proposed algorithm in evaluation of LOO CV scores could be much lower than that of a simple competing method. This also allows an efficient evaluation of the influence of the case on the fitted model as a function of ω . Different from case-deletion diagnostics (Cook, 1977; Belsley et al., 1980), Cook (1986) proposed analogous case-influence graphs to assess local influence of a statistical model. Using the case-weight adjusted solution path, we can generate case-influence graphs efficiently for penalized quantile regression and examine the influence of small perturbations of data on regression quantiles. In contrast to mean regression, it is observed that cases with almost identical case deletion statistics could have quite different case-influence graphs in quantile regression. Numerically, we observe that the data dimension and the value of the penalty parameter can influence the computational time of the algorithm.

The paper is organized as follows. Section 2 proposes a path-following algorithm for case-weight adjusted quantile regression with ridge penalty for cross validation. A formal validation of the algorithm is provided on the basis of the optimality conditions. Section 3 presents another application of the case-weight adjusted solutions for measuring case influence on regression quantiles. In Section 4, some numerical studies are presented to illustrate the applications of the proposed case-weight adjusted solution path algorithm and its favorable computational efficiency for computing LOO CV scores. In Section 5, we demonstrate the utility of the proposed method for analyzing real-world data by assessing

the case influence in quantile regression. We conclude with some remarks in Section 6. Technical proofs are provided in Appendix.

2 Case-weight Adjusted Solution Path in Quantile Regression with Ridge Penalty

In this section, we present a path-following algorithm for solving the penalized quantile regression problem in (2) with case-weight ω . We illustrate in detail how to construct a solution path from the full-data solution as the case-weight decreases from 1 to 0. As with many existing solution path algorithms, the key to our derivations is the optimality conditions for (2). We analyze the Karush-Kuhn-Tucker (KKT) conditions for the problem after reformulating it as a constrained optimization problem. We formally prove that the path generated by the proposed algorithm solves the problem (2), and is piecewise linear in ω .

2.1 Optimality Conditions

In the path-following algorithm, we start from the full-data solution at $\omega = 1$, and specify a scheme to update the solution as ω decreases from 1 to 0. The updating scheme is designed so that the path generated satisfies the KKT conditions for every ω in $[0, 1]$. The KKT

conditions for the optimization problem (2) are

$$X^\top \theta_\omega = \lambda \beta_\omega, \text{ and } \theta_\omega^\top \mathbf{1}_n = 0 \quad (3)$$

$$\theta_{i,\omega} = \begin{cases} \tau - 1 & \text{for } i \neq i^* \\ \omega(\tau - 1) & \text{for } i = i^* \end{cases} \quad \text{if } y_i - \beta_{0,\omega} - x_i^\top \beta_\omega < 0 \quad (4)$$

$$\theta_{i,\omega} \in \begin{cases} [\tau - 1, \tau] & \text{for } i \neq i^* \\ [\omega(\tau - 1), \omega\tau] & \text{for } i = i^* \end{cases} \quad \text{if } y_i - \beta_{0,\omega} - x_i^\top \beta_\omega = 0 \quad (5)$$

$$\theta_{i,\omega} = \begin{cases} \tau & \text{for } i \neq i^* \\ \omega\tau & \text{for } i = i^* \end{cases} \quad \text{if } y_i - \beta_{0,\omega} - x_i^\top \beta_\omega > 0 \quad (6)$$

where $(\beta_{0,\omega}, \beta_\omega)$ denotes the solution of (2), $\theta_\omega = (\theta_{1,\omega}, \dots, \theta_{n,\omega}) \in \mathbb{R}^n$ is the set of dual variables associated with the residual bounds, $X = (x_1, \dots, x_n)^\top \in \mathbb{R}^{n \times p}$ is the $n \times p$ design matrix, and $\mathbf{1}_n$ is the vector of n ones. A detailed derivation of the KKT conditions is included in the Appendix A.1. The solution $(\beta_{0,\omega}, \beta_\omega)$ and θ_ω can thus be determined by the equality conditions in (3)–(6).

2.2 Outline of the Solution Path Algorithm

Let $r_{i,\omega} = y_i - \beta_{0,\omega} - x_i^\top \beta_\omega$ denote the residual for the i th case with $(\beta_{0,\omega}, \beta_\omega)$. According to the sign of each residual, we can partition the n cases into three sets. Depending on which side of 0 each residual falls on, the three sets are called the elbow set, $\mathcal{E}_\omega = \{i : r_{i,\omega} = 0\}$, the left set of the elbow, $\mathcal{L}_\omega = \{i : r_{i,\omega} < 0\}$ and the right set of the elbow, $\mathcal{R}_\omega = \{i : r_{i,\omega} > 0\}$. The three sets may evolve as ω decreases. We call ω_m a breakpoint if the three sets change at ω_m . The following rules specify how and when we should update the three sets at each breakpoint:

- (a) if $\theta_{i,\omega} = \tau[\omega + (1 - \omega)\mathbb{I}(i \neq i^*)]$ for some $i \in \mathcal{E}_\omega$, then move case i from \mathcal{E}_ω to the right set of the elbow \mathcal{R}_ω . Here $\mathbb{I}(\cdot)$ is the indicator function for a condition, which takes the value 1 if the condition is met, and 0 otherwise.

(b) if $\theta_{i,\omega} = (\tau - 1)[\omega + (1 - \omega)\mathbb{I}(i \neq i^*)]$ for some $i \in \mathcal{E}_\omega$, then move case i from \mathcal{E}_ω to the left set of the elbow \mathcal{L}_ω .

(c) if $r_{i,\omega} = 0$ for some $i \in \mathcal{L}_\omega \cup \mathcal{R}_\omega$, then move case i from $\mathcal{L}_\omega \cup \mathcal{R}_\omega$ to the elbow set \mathcal{E}_ω .

Given the three sets, we next analyze how the solution should evolve between two breakpoints. Toward this end, we let $\{\omega_m, \text{ for } m = 0, 1, \dots, M \mid 0 \leq \omega_M < \dots < \omega_1 < \omega_0 = 1\}$ be the set of breakpoints, and denote by $\mathcal{E}_m, \mathcal{L}_m$ and \mathcal{R}_m the three sets between ω_{m+1} and ω_m for $m = 1, \dots, M$. Note that we have abbreviated $\mathcal{E}_{\omega_m}, \mathcal{L}_{\omega_m}$ and \mathcal{R}_{ω_m} to $\mathcal{E}_m, \mathcal{L}_m$ and \mathcal{R}_m , respectively. Now, when $\omega_{m+1} < \omega < \omega_m$, the KKT conditions determine how $(\beta_{0,\omega}, \beta_\omega)$ and θ_ω should change as functions of ω and we can show that they satisfy the following:

$$\begin{aligned} -\sum_{i \in \mathcal{E}_m} \theta_{i,\omega} &= \sum_{i \notin \mathcal{E}_m} \theta_{i,\omega} \\ \lambda \beta_\omega - \sum_{i \in \mathcal{E}_m} \theta_{i,\omega} x_i &= \sum_{i \notin \mathcal{E}_m} \theta_{i,\omega} x_i \\ \beta_{0,\omega} + x_i^\top \beta_\omega &= y_i \quad \text{for } i \in \mathcal{E}_m \end{aligned} \tag{7}$$

using (3) and (5), and the fact that $\theta_{i,\omega} = \{\tau - \mathbb{I}(i \in \mathcal{L}_m)\}\{\omega + (1 - \omega)\mathbb{I}(i \neq i^*)\}$ for $i \notin \mathcal{E}_m$ from (4) and (6).

Next, we show that $(\beta_{0,\omega}, \beta_\omega, \theta_\omega)$ satisfying (7) must be linear in ω . Before proceeding, we introduce some notations. For any vector $v = (v_1, \dots, v_n)^\top \in \mathbb{R}^n$ and any index set $A = \{i_1, \dots, i_k\} \subseteq \{1, 2, \dots, n\}$, define $v_A = (v_{i_1}, \dots, v_{i_k})$ be a sub-vector of v . Similarly, for any matrix $M = (m_1, \dots, m_n)^\top \in \mathbb{R}^{n \times L}$, let $M_A = (m_{i_1}, \dots, m_{i_k})^\top$ be a submatrix of M , where m_i^\top is the i th row of M for $i = 1, \dots, n$. Let $\mathbf{0}_k$ be the vector of k zeros and \mathbf{O}_k be the $k \times k$ matrix of zeros. Now we can rewrite (7) into a matrix form:

$$\begin{pmatrix} 0 & \mathbf{0}_p^\top & -\mathbf{1}_{\mathcal{E}_m}^\top \\ 0 & \lambda I_p & -X_{\mathcal{E}_m}^\top \\ \mathbf{1}_{\mathcal{E}_m} & X_{\mathcal{E}_m} & \mathbf{O}_{|\mathcal{E}_m|} \end{pmatrix} \begin{pmatrix} \beta_{0,\omega} \\ \beta_\omega \\ \theta_{\mathcal{E}_m,\omega} \end{pmatrix} = \begin{pmatrix} \mathbf{1}_{\mathcal{L}_m}^\top \theta_{\mathcal{L}_m} + \mathbf{1}_{\mathcal{R}_m}^\top \theta_{\mathcal{R}_m} \\ X_{\mathcal{L}_m}^\top \theta_{\mathcal{L}_m} + X_{\mathcal{R}_m}^\top \theta_{\mathcal{R}_m} \\ y_{\mathcal{E}_m} \end{pmatrix},$$

which is a system of linear equations of dimension $1 + p + |\mathcal{E}_m|$. $\mathbf{1}_{\mathcal{E}_m}$ is defined from $\mathbf{1}_n$, and I_p is the $p \times p$ identity matrix. Note that the left hand side of the above linear equation

does not depend on ω , while the right hand side is a linear function of ω . This implies that its solution must be a linear function of ω . The following lemma summarizes the properties of the solution path described thus far.

Lemma 1. *The solution path $(\beta_{0,\omega}, \beta_\omega)$ satisfying the KKT conditions (3)–(6) is piecewise linear in ω .*

Using Lemma 1, we propose a solution path algorithm that updates the three sets following the aforementioned rules at each breakpoint and linearly updates the solutions between two consecutive breakpoints. First we provide an outline of our algorithm:

- Start with the full-data solution at $\omega = 1$.
- While $\omega > 0$,
 - (i) Decrease ω and update $(\beta_{0,\omega}, \beta_\omega)$ and θ_ω until one of the inequalities in the KKT conditions is violated.
 - (ii) When the violation happens, update the three sets according to the rules (a)–(c). Then go back to Step (i).

2.3 Determining Breakpoints

For implementation of Step (i), we need to derive a formula for the next breakpoint ω_{m+1} among $\omega \leq \omega_m$. From the KKT conditions (3)–(6), we can see that as ω decreases, the conditions (4)–(6) will be violated when $\theta_{i,\omega} = \tau[\omega + (1 - \omega)\mathbb{I}(i \neq i^*)]$ or $(\tau - 1)[\omega + (1 - \omega)\mathbb{I}(i \neq i^*)]$ for some $i \in \mathcal{E}_m$, or $r_{i,\omega} = 0$ for some $i \in \mathcal{L}_m \cup \mathcal{R}_m$. Thus, to find the next breakpoint ω_{m+1} , we need to derive how $\theta_{\mathcal{E}_m,\omega}$ and $r_\omega = (r_{1,\omega}, \dots, r_{n,\omega})$ change as functions of ω . This is established in the following proposition, for which we need to impose an assumption that any $\min(p + 2, n)$ points of $\{(\tilde{x}_i, y_i)\}_{i=1}^n$ are linearly independent, where $\tilde{x}_i = (1, x_i^\top)^\top$. We call this condition the *general position condition*. A similar condition is also imposed in Li et al. (2007).

Proposition 1. *Suppose that the data points $\{(\tilde{x}_i, y_i)\}_{i=1}^n$ satisfy the general position condition. Then the solution path for (2) satisfies the following properties:*

I. *When $i^* \in \mathcal{R}_m \cup \mathcal{L}_m$, we have that*

$$\theta_{\mathcal{E}_m, \omega} - \theta_{\mathcal{E}_m, \omega_m} = b_m(\omega - \omega_m), \quad (8)$$

where

$$b_m = -(\tilde{X}_{\mathcal{E}_m} \tilde{X}_{\mathcal{E}_m}^\top)^{-1} \left[b_{0,m} \mathbf{1}_{\mathcal{E}_m} + \tilde{X}_{\mathcal{E}_m} \tilde{x}_{i^*} (\tau - \mathbb{I}(i^* \in \mathcal{L}_m)) \right] \quad (9)$$

$$\text{with } b_{0,m} = \frac{1 - \mathbf{1}_{\mathcal{E}_m}^\top (\tilde{X}_{\mathcal{E}_m} \tilde{X}_{\mathcal{E}_m}^\top)^{-1} \tilde{X}_{\mathcal{E}_m} \tilde{x}_{i^*}}{\mathbf{1}_{\mathcal{E}_m}^\top (\tilde{X}_{\mathcal{E}_m} \tilde{X}_{\mathcal{E}_m}^\top)^{-1} \mathbf{1}_{\mathcal{E}_m}} (\tau - \mathbb{I}(i^* \in \mathcal{L}_m)), \quad (10)$$

and

$$\lambda(r_\omega - r_{\omega_m}) = h_m(\omega - \omega_m), \quad (11)$$

where

$$h_m = -b_{0,m} \mathbf{1} - \tilde{X} \left[\tilde{X}_{\mathcal{E}_m}^\top b_m + \{\tau - \mathbb{I}(i^* \in \mathcal{L}_m)\} \tilde{x}_{i^*} \right]. \quad (12)$$

II. *Moreover, $i^* \in \mathcal{E}_m$ can only happen when $m = 0$, and if that happens, both r_ω and θ_ω are constant vectors for $\omega \in [\omega_1, 1]$, and i^* will move from \mathcal{E}_0 to $\mathcal{L}_1 \cup \mathcal{R}_1$ at the next breakpoint $\omega_1 = \frac{\theta_{i^*, \omega_0}}{\tau - \mathbb{I}(\theta_{i^*, \omega_0} < 0)}$, and stay in $\mathcal{L}_m \cup \mathcal{R}_m$ for all $m = 1, \dots, M$.*

The proof of Proposition 1 is provided in the Appendix. Using Proposition 1, we can easily determine the next breakpoint if $i^* \in \mathcal{L}_m \cup \mathcal{R}_m$. Specifically, the next breakpoint is determined by the largest $\omega < \omega_m$ such that $\theta_{i, \omega} = \tau$ or $\tau - 1$ for some $i \in \mathcal{E}_m$, or $r_{i, \omega} = 0$ for some $i \in \mathcal{L}_m \cup \mathcal{R}_m$. Hence, the next breakpoint is

$$\omega_{m+1} = \max(\omega_{1,m+1}, \omega_{2,m+1}), \quad (13)$$

where $\omega_{1,m+1}$ is the largest $\omega < \omega_m$, at which $\theta_{i, \omega}$, for some $i \in \mathcal{E}_m$, hits either of the boundaries τ or $\tau - 1$, and $\omega_{2,m+1}$ is the largest $\omega < \omega_m$, at which $r_{i, \omega}$ hits 0 for some

$i \in \mathcal{L}_m \cup \mathcal{R}_m$. Moreover, we know that $\theta_{\mathcal{E}_m, \omega}$ and r_ω evolve as linear functions of ω according to (8) and (11), from which we obtain the following for $\omega_{1,m+1}$ and $\omega_{2,m+1}$:

$$\omega_{1,m+1} = \max_{\theta \in \{\tau, \tau-1\}} \left(\max_{i \in \mathcal{E}_m \text{ and } -\omega_m \leq \frac{\theta - \theta_{i, \omega_m}}{b_{i,m}} < 0} \frac{\theta - \theta_{i, \omega_m}}{b_{i,m}} + \omega_m \right) \quad (14a)$$

$$\omega_{2,m+1} = \max_{i \in \mathcal{L}_m \cup \mathcal{R}_m \text{ and } 0 < \frac{\lambda r_{i, \omega_m}}{h_{i,m}} \leq \omega_m} - \frac{\lambda r_{i, \omega_m}}{h_{i,m}} + \omega_m, \quad (14b)$$

where $b_{i,m}$ and $h_{i,m}$ are the i th component of slopes b_m and h_m defined in (9) and (12), respectively. From these two formulas, we can see that the next breakpoint can be determined without evaluating the solutions between two breakpoints.

2.4 A Path-Following Algorithm

We summarize the detailed description of our proposed solution-path algorithm in Algorithm 1 in the Appendix. The following theorem states that the path generated by Algorithm 1 is indeed a solution path to the optimization problem (2), provided that the data points satisfy the general position condition.

Theorem 1. *Assume that the set of data points $\{(\tilde{x}_i, y_i)\}_{i=1}^n$ satisfies the general position condition. The case-weight adjusted path generated by Algorithm 1 solves the optimization problem (2) indexed by $\omega \in [0, 1]$.*

3 Case Influence Assessment in Quantile Regression

In addition to model validation through LOO CV, the case-weight adjusted solution path for quantile regression can be used for assessing case influences on regression quantiles. In this section, we further explore the use of the case-weight adjusted solutions for measuring case influence.

In statistical modeling, assessing case influence and identifying influential cases is crucial for model diagnostics. Assessment of case influence on a statistical model has been

extensively studied in robust statistics literature. Seminal works on case-influence assessment include [Cook \(1977\)](#), [Cook \(1979\)](#) and [Cook and Weisberg \(1982\)](#). As a primary example, Cook proposed the following measure, known as Cook’s distance for case i^* :

$$D_{i^*} = \frac{\sum_{i=1}^n (\hat{f}(x_i) - \hat{f}^{[-i^*]}(x_i))^2}{p\hat{\sigma}^2},$$

where $\hat{\sigma}^2$ is an estimate of the error variance in a regression model $y_i = f(x_i) + \epsilon_i$ with $\epsilon_i \sim N(0, \sigma^2)$. Cook’s distance measures an aggregated effect of one single case on n fitted values after that case is deleted. In other words, it compares two sets of fitted values when case i^* has weight $\omega = 1$ and $\omega = 0$. In contrast to the standard Cook’s distance, [Cook \(1986\)](#) also introduced the notion of a case-influence graph to get a broad view of case influence as a function of the case-weight ω . As a general version of D_{i^*} , a case-weight adjusted Cook’s distance is defined as

$$D_{i^*}(\omega) = \frac{\sum_{i=1}^n (\hat{f}(x_i) - \hat{f}_\omega^{i^*}(x_i))^2}{p\hat{\sigma}^2} \tag{15}$$

for each $\omega \in [0, 1]$, where $\hat{f}_\omega^{i^*}$ is the fitted model when case i^* has weight ω and the remaining cases have weight 1. When $\omega = 0$, $\hat{f}_0^{i^*}$ coincides with $\hat{f}^{[-i^*]}$ and thus $D_{i^*}(0) = D_{i^*}$. With this generalized distance, we could examine more complex modes of case influence that may not be easily detected by Cook’s distance D_{i^*} . [Figure 3](#) provides an example of case-influence graphs where two cases A and B have the same Cook’s distance but obviously different influence on the model fit depending on ω . Two cases A and B can be treated the same if merely assessed by D_{i^*} , but since $D_A(\omega) \geq D_B(\omega)$ at each $\omega \in [0, 1]$, case A should be treated as more influential than case B.

Case-influence graphs provide comprehensive information on local influence of cases in general, and they can be used to assess the differences in robustness of modeling procedures. However, generation of such graphs is computationally more expensive than Cook’s distance. To circumvent the computational issue, [Cook \(1986\)](#) suggested to focus on the local influence around $\omega = 1$ through the curvature of the graph. As evident in (15),

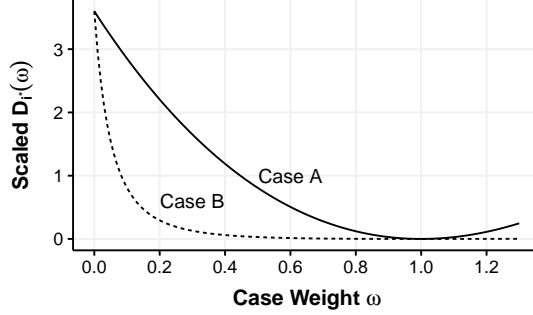


Figure 3: An illustrative example of case-influence graphs in least squares regression based on Figure 1 in Cook (1986).

once $\hat{f}_\omega^{i^*}$ is obtained, the generalized Cook’s distance $D_{i^*}(\omega)$ is readily available. Thus, using path-following algorithms that generate case-weight adjusted solutions, we can easily construct case-influence graphs without additional computational cost.

Leveraging our solution path algorithm for quantile regression with adjusted case-weight, we specifically study the characteristics of case-influence graphs for various quantiles. In addition, we include case-influence graphs of ridge regression for comparison of mean regression and quantile regression as a robust counterpart in terms of case influences. For ridge regression with penalty parameter λ and case-weight ω for case $i^* \in \{1, \dots, n\}$, we solve the following problem:

$$\underset{\beta_0 \in \mathbb{R}, \beta \in \mathbb{R}^p}{\text{minimize}} \sum_{i \neq i^*} (y_i - \beta_0 - x_i^\top \beta)^2 + \omega (y_{i^*} - \beta_0 - x_{i^*}^\top \beta)^2 + \lambda \|\beta\|_2^2. \quad (16)$$

With squared error loss, the case-weight adjusted fit $\hat{f}_\omega^{i^*}$ can be computed in closed form and, thus, obtaining $D_{i^*}(\omega)$ is straightforward for ridge regression. For quantile regression with the check loss, however, $\hat{f}_\omega^{i^*}$ cannot be obtained as easily, but our proposed solution path algorithm readily offers the path for $D_{i^*}(\omega)$ as ω decreases from 1 to 0.

We present the case-weight adjusted Cook’s distance $D_{i^*}(\omega)$ for ridge regression in the following proposition. Let $H(\lambda) = \tilde{X}(\tilde{X}^\top \tilde{X} + \lambda \tilde{I})^{-1} \tilde{X}^\top$ denote the hat matrix for ridge

regression with full data, where $\tilde{I} = \begin{pmatrix} 0 \\ I \end{pmatrix}$. $h_{ij}(\lambda)$ denotes the ij th entry of $H(\lambda)$ and $h_{ii}(\lambda)$ is the leverage of case i in ridge regression.

Proposition 2. *For ridge regression with penalty parameter λ ,*

$$D_{i^*}(\omega) = \frac{r_{i^*}^2 \sum_{j=1}^n h_{ji^*}^2(\lambda)}{p\hat{\sigma}^2 \{1/(1-\omega) - h_{i^*i^*}(\lambda)\}^2}, \quad (17)$$

where r_{i^*} is the residual for case i^* from the full data fit.

The proposition above shows that $D_{i^*}(\omega)$ for ridge regression is smooth and convex in ω . The convexity comes from the fact that the second derivative of $g_h(\omega) = \{1/(1-\omega) - h\}^{-2}$ for a positive constant h is $\{2 + 4h(1-\omega)\}\{1 - h(1-\omega)\}^{-4}$, which is positive for $\omega \in (0, 1)$. Furthermore, $g_h(\omega)$ with $h \in [0, 1]$ decreases monotonically in $\omega \in (0, 1)$ since $1/(1-\omega)$ increases in ω and $1/(1-\omega) - h > 0$. This implies that as the case-weight ω decreases from 1 to 0, $D_{i^*}(\omega)$ increases monotonically since $h_{i^*i^*} \in [0, 1]$. When both $\omega = 0$ and $\lambda = 0$, $D_{i^*}(\omega)$ reduces to standard Cook's distance $(r_{i^*}^2 h_{i^*i^*}) / \{p\hat{\sigma}^2(1 - h_{i^*i^*})^2\}$, where $h_{i^*i^*}$ is the leverage of case i^* in ordinary linear regression. This can be seen from the fact that $\sum_{j=1}^n h_{i^*j}^2(\lambda)$ is the i^* th diagonal entry of $H^2(\lambda)$ and $H(0)$ is idempotent.

For penalized quantile regression, the piecewise linear solution path that we have constructed suggests that the discrepancy between the full-data fit and the case-weight adjusted fit at any ω , $\hat{f}(x_i) - \hat{f}_\omega^{i^*}(x_i)$, is also piecewise linear, and thus $D_{i^*}(\omega)$ is piecewise quadratic in ω . Hence, $D_{i^*}(\omega)$ can be easily obtained by aggregating the piecewise squared difference in the fit from 1 to ω . Equivalently, using (12), the squared difference in the residual, $(r_i - r_{i,\omega})^2$, can be aggregated to produce $D_{i^*}(\omega)$. An explicit expression of $D_{i^*}(\omega)$ is provided in the proposition below.

Proposition 3. *For penalized quantile regression in (2) with penalty parameter λ , if $\omega \in$*

$(\omega_{m+1}, \omega_m]$,

$$\begin{aligned}
D_{i^*}(\omega) &= \frac{1}{p\hat{\sigma}^2} \sum_{i=1}^n (\hat{f}(x_i) - \hat{f}_\omega^{i^*}(x_i))^2 = \frac{1}{p\hat{\sigma}^2} \sum_{i=1}^n (r_{i,\omega} - r_{i,\omega_0})^2 \\
&= \frac{1}{p\hat{\sigma}^2} \|\mathbf{r}_\omega - \mathbf{r}_{\omega_m} + \sum_{k=1}^m (\mathbf{r}_{\omega_k} - \mathbf{r}_{\omega_{k-1}})\|_2^2 \\
&= \frac{1}{p\hat{\sigma}^2} \|(\omega - \omega_m)\mathbf{h}_m + \sum_{k=1}^m (\omega_k - \omega_{k-1})\mathbf{h}_{k-1}\|_2^2, \tag{18}
\end{aligned}$$

where \mathbf{h}_k is the vector of the slopes of the case-weight adjusted residuals \mathbf{r} over $(\omega_{k+1}, \omega_k]$.

Numerical examples of case-influence graphs for ridge regression and quantile regression are presented in Section 4.

4 Numerical Studies

In this section, we present various numerical studies to illustrate the applications of our proposed case-weight adjusted solution path algorithm, including LOO CV and case-influence graphs. We also analyze the computational complexity of the proposed path-following algorithm, and demonstrate its efficiency in computation of LOO CV scores numerically. Throughout the numerical studies, the standard linear model $y_i = \beta_0 + x_i^\top \beta + \epsilon_i$ was used. We independently generated covariates $\{x_{ij} : i = 1, \dots, n, j = 1, \dots, p\}$, coefficients $(\beta_0, \beta_1, \dots, \beta_p)$ and random errors $\{\epsilon_i : i = 1, \dots, n\}$ from the standard normal distribution. We also created an R package *NonsmoothPath* that can be used to reproduce the numerical results in this section. The R package is available at <https://github.com/qiuyu1995/NonsmoothPath>.

4.1 Leave-One-Out CV

We first investigate the inaccuracy of GACV in approximating LOO CV scores as demonstrated in the introduction for extreme quantiles. This necessitates exact LOO CV. Then we numerically show that resorting to the homotopy strategy and applying our proposed

ω path algorithm to obtain all the LOO solutions directly from the full-data solution could be more scalable and efficient than a straightforward procedure of solving n LOO problems separately.

4.1.1 Comparison between GACV and exact LOO CV

The exact LOO CV score in quantile regression is defined as $RCV(\lambda) = \frac{1}{n} \sum_{i=1}^n \rho_\tau(y_i - \hat{f}_\lambda^{[-i]}(x_i))$ and GACV score from Li et al. (2007) is defined as $GACV(\lambda) = \frac{1}{n-|\mathcal{E}_\lambda|} \sum_{i=1}^n \rho_\tau(y_i - \hat{f}(x_i))$. We set $n = 50$, $p = 30$, and $N_\lambda = 100$ to compare the exact LOO CV and GACV scores at various quantiles, $\tau = 0.5, 0.3, 0.1$, and 0.01 . Figure 2 reveals that as the pre-specified quantile τ gets extreme, the quality of GACV deteriorates. Similar observations have been made in the empirical studies of Li et al. (2007) and Reiss and Huang (2012).

GACV is based on the smoothed check loss, $\rho_{\tau,\delta}$, with a small threshold δ , which is given by $\rho_{\tau,\delta}(r) = (\tau I(r > 0) + (1 - \tau)I(r < 0))r^2/\delta$. This approximate loss differs from ρ_τ only in the region of $(-\delta, \delta)$. In the derivation of GACV, the following first-order Taylor expansion of the smoothed loss is used: $\rho_\tau(y_i - \hat{f}^{[-i]}(x_i)) - \rho_\tau(y_i - \hat{f}(x_i)) \approx \rho'_{\tau,\delta}(y_i - \hat{f}(x_i))(\hat{f}(x_i) - \hat{f}^{[-i]}(x_i))$, which may be attributed to the issue with GACV. Letting $r_i^{[-i]} = y_i - \hat{f}^{[-i]}(x_i)$, the LOO prediction error, and $r_i = y_i - \hat{f}(x_i)$, the residual from the full data fit, we define the approximation error of GACV from the exact LOO CV as

$$\Delta_{\text{approx.}} := \rho'_{\tau,\delta}(r_i)(r_i^{[-i]} - r_i) - [\rho_\tau(r_i^{[-i]}) - \rho_\tau(r_i)]. \quad (19)$$

Apparently the approximation error only comes from points with different signs of $r_i^{[-i]}$ and r_i . We categorize all the possible scenarios for the approximation error in Table 1 in the Appendix except the case when $r_i^{[-i]} = 0$. In the case of $r_i^{[-i]} = 0$, the approximation error is negligible.

When the residual r_i and the LOO residual $r_i^{[-i]}$ have different signs (+, 0, -), we call the case *flipped* as in scenarios (b) and (d) in Table 1. Potential issues with GACV for extreme quantiles are summarized as follows:

- (i) The cases in the elbow set have zero residuals. Thus, those cases are almost always flipped. In fact, in our experiment, we found that all the *flipped* cases belong to the elbow set. The derivative of the smoothed check loss at $r_i = 0$ for the approximation is zero while the corresponding derivative for the true difference is either τ or $\tau - 1$. This leads to the approximation error listed in scenarios (b) and (d).
- (ii) For scenarios (b) and (d), the approximation error $\Delta_{\text{approx.}}$ depends on both τ and $r_i^{[-i]}$. Given $r_i^{[-i]}$, extreme values of τ (e.g., $\tau = 0.01$ in Figure 2) lead to a larger approximation error in scenario (d), in particular. To see the effect of τ on the discrepancy between the true difference and its approximation, we examine the distribution of the LOO residuals $r_i^{[-i]}$ for flipped cases. Figure 4 displays the distribution of $r_i^{[-i]}$ for *flipped* cases for various quantiles when $\log(\lambda) = -6$ from Figure 2. As τ becomes more extreme, the distribution tends to be more left-skewed, and scenario (d) occurs more often than scenario (b). This results in larger discrepancy between LOO CV and GACV for extreme quantiles as illustrated in Figure 2.

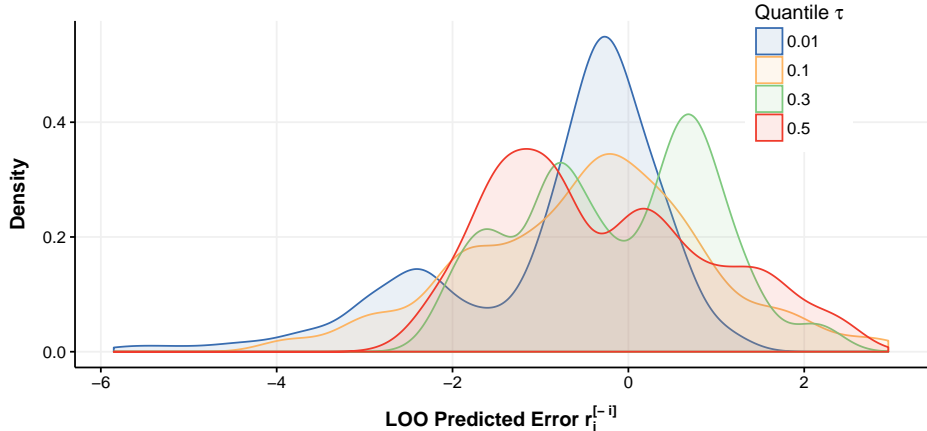


Figure 4: The distributions of LOO residual $r_i^{[-i]}$ for *flipped* cases for various quantiles ($\tau = 0.5, 0.3, 0.1, \text{ and } 0.01$).

4.1.2 Computation for Exact Leave-One-Out CV

We compare two approaches to computing exact LOO CV scores over a set of N_λ pre-specified grid points for the tuning parameter λ . The first one is based on the proposed ω -path algorithm in Algorithm 1. The other one applies the “ λ -path” algorithm proposed in Li et al. (2007) to the n LOO data sets separately. We make comparisons of the two approaches in terms of theoretical computational complexity as well as practical runtime on simulated data sets.

We first analyze the computational complexity of applying the “ λ -path” algorithm proposed in Li et al. (2007) n times. Note that the λ -path algorithm of Li et al. (2007) generates the solution path as λ decreases from ∞ to 0. The computation of the exact LOO CV scores involves two components: (i) applying this algorithm to each of the n LOO data sets; and (ii) linearly interpolating the solutions between consecutive grid points. According to Li et al. (2007), the average cost of computing one λ path is $O(n^2p)$ and the cost for the linear interpolation is $O(N_\lambda p)$. Hence, the total cost of computing the exact LOO CV scores in this case is $O(np(n^2 + N_\lambda))$.

For the proposed ω -path algorithm, it generates each LOO solution directly from the full-data solution. The computation consists of generating n case-weight adjusted ω -paths, whose cost depends on the number of breakpoints for the case-weight parameter ω . To simplify the analysis, we work with the average number of ω -breakpoints, denoted by N_ω . Our empirical studies show that N_ω is usually small compared to problem dimension (see Table 2 in the Appendix). In fact, for large values of λ , we can prove that $N_\omega = 1$. Therefore, we assume that $N_\omega = O(1)$ in our analysis. By inspecting Algorithm 1, the average computational cost at each ω -breakpoint is dominated by Line 15, which computes $b_{0,m}$, b_m , and h_m —the slopes of $\beta_{0,\omega}$, $\theta_{\mathcal{E},\omega}$, and r_ω . First, the computation of $b_{0,m}$ and b_m in (9) and (10) involves inverting a $|\mathcal{E}_m| \times |\mathcal{E}_m|$ matrix $\tilde{X}_{\mathcal{E}_m} \tilde{X}_{\mathcal{E}_m}^\top$, which typically costs $O(|\mathcal{E}_m|^3)$. This can be reduced further to $O(|\mathcal{E}_m|^2)$ by employing a rank-one updating algorithm (Hager, 1989). Moreover, the cost for computing h_m in (12) is $O(np)$. Therefore, the average cost of generating one ω -path at a grid point for λ is $O(N_\omega(np + |\mathcal{E}_m|^2)) = O(np)$,

because $|\mathcal{E}_m| \leq \min(n, p + 1)$ according to Lemma 2 in Appendix and the assumption that $N_\omega = O(1)$. Consequently, the average cost of computing exact LOO CV scores over N_λ grid points using the proposed ω -path algorithm is $O(N_\lambda n^2 p)$, which is in contrast to the cost of the λ -path algorithm, $O(np(n^2 + N_\lambda))$. Note that the savings could be large when $N_\lambda \ll n$, which is corroborated by an empirical runtime comparison.

We present numerical examples comparing the actual runtime performance of the two algorithms. Both algorithms are implemented in C++ with Armadillo package, and were run on a Linux cluster with 24 cores and 128 GB of memory per node. We varied the quantile ($\tau = 0.1, 0.3, 0.5$), sample size ($n = 50$ to 300), number of covariates ($p = 50$ to 300), and number of grid points ($N_\lambda = 20, 50$). The grid points for λ were equally spaced on the logarithmic scale over the range of λ -breakpoints for the full data fit. For each setting, we had 20 independent replicates and the results are summarized over the replicates. To see the complexity of ω -paths clearly, we recorded the average number of ω -breakpoints when N_λ is 50 in Table 2.

The runtimes for computation of CV scores depend on the number of grid points and generally a grid for the tuning parameter needs a sufficiently fine resolution to locate the minimum CV score. Figure 5 illustrates that both $N_\lambda = 20$ and 50 are adequate for identifying the optimal tuning parameter value for λ . The solid curves are the complete CV score curves while the dots on the curves correspond to the CV scores at the grid points. The minimizers of the CV scores over the grid points are indicated by the solid vertical lines in the two panels, both of which are close to the dashed vertical lines which correspond to the minimizers of the complete CV score curves.

The runtime comparisons are presented in Figure 6 for $p < n$ settings and Figure 7 for $p > n$ settings. The figures are based on the numerical summaries of the results in Tables 3 and 4 in Appendix. Overall, they show that as the sample size n increases, our proposed ω -path algorithm becomes more scalable than the competing λ -path algorithm. This is consistent with our earlier analysis of computational complexities.

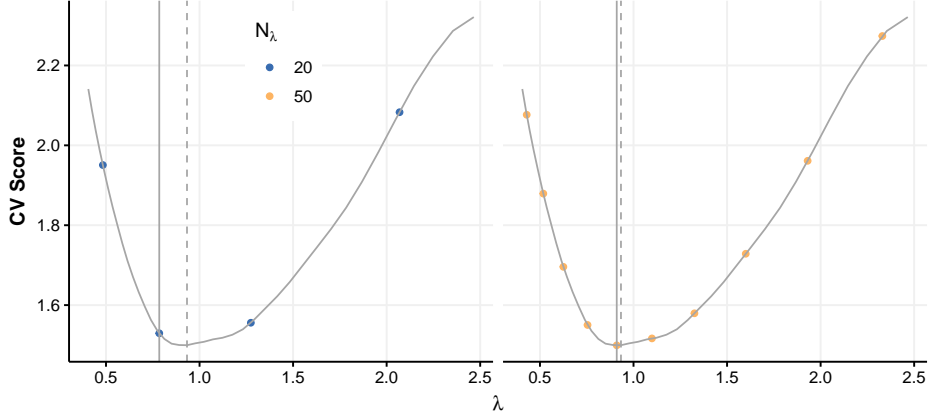


Figure 5: Comparison of two levels of grid resolution in cross validation ($n = 100, p = 100, \tau = 0.5$). The solid curve is a complete CV score curve zoomed in the basin around the optimal λ , and the dots on the curves are CV scores at the grid points with $N_\lambda = 20$ in the left panel and $N_\lambda = 50$ in the right panel.

4.2 Case-Influence Graphs

This section presents case-influence graphs for ridge regression and ℓ_2 -penalized quantile regression with the same data. As is introduced in Section 3, case-influence graphs show a broad view of the influence of a case on the model as a function of the case-weight ω . For simplicity, we rescale the generalized Cook's distance $D_{i^*}(\omega)$ in (15) by replacing the factor $1/p\hat{\sigma}^2$ with $1/n$ as

$$\tilde{D}_{i^*}(\omega) = \frac{1}{n} \sum_{i=1}^n (\hat{f}(x_i) - \hat{f}_\omega^{i^*}(x_i))^2. \quad (20)$$

Figures 8 and 9 provide case-influence graphs for ridge regression and penalized quantile regression using the same data. Here we remark some major differences in the characteristics of the graphs. As is discussed in Section 3, the influence graphs for ridge regression in Figure 8 are smooth, convex and monotonically decreasing in ω , while those for quantile regression in Figure 9 are piecewise quadratic. Moreover, there are few crossings in the curves for ridge regression in Figure 8, suggesting that the standard Cook's distance may well be adequate for assessing case influences in ridge regression. By contrast, Figure 9 reveals that for quantile regression, the relation between the case-influence graphs and case-

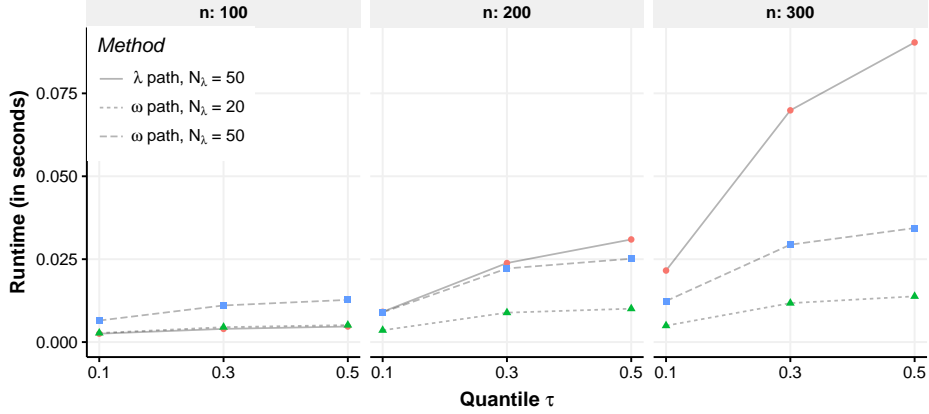


Figure 6: Comparison of the runtime per case (i.e., the total runtime/ n) between the ω -path and λ -path algorithms with different data dimensions, quantiles, and levels of grid resolution ($p = 50$; $n = 100, 200, \text{ and } 300$; $\tau = 0.1, 0.3, \text{ and } 0.5$; $N_\lambda = 20 \text{ and } 50$).

deletion statistics is more complex and some cases in the elbow set with almost identical standard Cook’s distance can have quite different influence on the model fit.

Additionally, the bold curves marked in Figures 8 and 9 show that for ridge regression, the cases with the most positive or negative full-data residuals have the greatest influence on the model fit, while for quantile regression that is not the case. In fact, for ridge regression, (17) in Proposition 2 implies strong dependence of the case influence on the magnitude of full-data residual. Without much heterogeneity in the case leverages as in our data setting, the cases with the most positive or negative full-data residuals would have the greatest influence. However, for quantile regression, the form of Cook’s generalized distance derived in (18) does not reveal any specific relation between case influence and the magnitude of full-data residual. It is observed that the residuals for the cases with the most positive or negative values tend not to change their signs as ω decreases from 1 to 0, and thus those cases are unlikely to enter the elbow set. They may have little influence on the model fit because the estimated coefficients $(\hat{\beta}_{0,\omega}, \hat{\beta}_\omega)$ only depend on the responses in the elbow set $y_{\mathcal{E}_m}$ along with $X_{\mathcal{E}_m}$ as shown in Section 2. This is akin to the fact that sample quantiles for modest τ are not affected by extreme observations. The case-influence graphs for quantile regression confirm this expectation, providing another perspective on

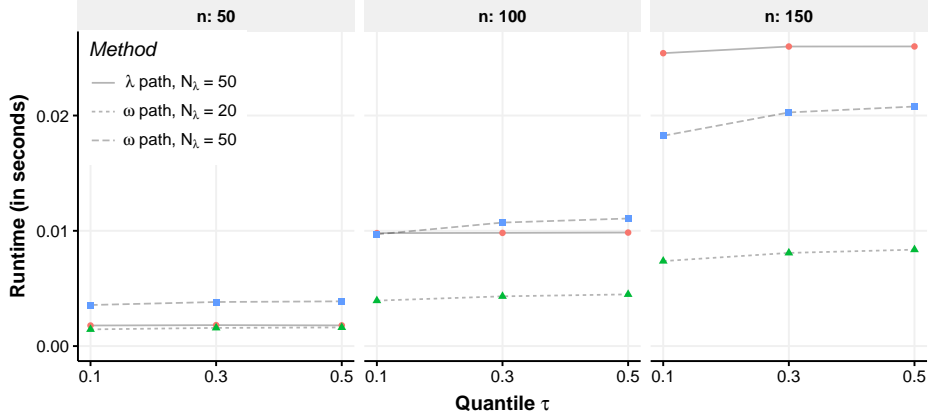


Figure 7: Comparison of the runtime per case between the ω -path and λ -path algorithms with different data dimensions, quantiles and levels of grid resolution ($p = 300$; $n = 50, 100$ and 150 ; $\tau = 0.1, 0.3$, and 0.5 ; $N_\lambda = 20$ and 50).

the robustness of quantile regression for modest regression quantiles. Overall, the elbow set points are relatively more critical across different target quantiles while the left elbow points tend to be more influential for small quantiles ($\tau = 0.3$ and 0.1) in Figure 9. Similar observations will be made in the data analysis presented in the next section.

5 Data Analysis

We illustrate how the proposed case-weight adjusted solution path and the corresponding case-influence graph can be utilized in real-life applications using the King County house sales data. By examining Cook’s distance as a case deletion statistic (i.e., $D_{i^*}(0)$ in (15) of Section 3), we demonstrate how the proposed methods can help identify influential observations in quantile regression. For normalization of Cook’s distance, we used a robust estimate of the error variance σ^2 based on the median absolute deviation from the median regression.

The King County house sales data, publicly available on [Kaggle](#), includes the price and property information of homes sold in King County, WA, between May 2014 and May 2015. Following the exploratory analysis in [Luan et al. \(2022\)](#), we selected 12 features for an l_2 -penalized quantile regression, and used a random sample of $n = 200$ houses for

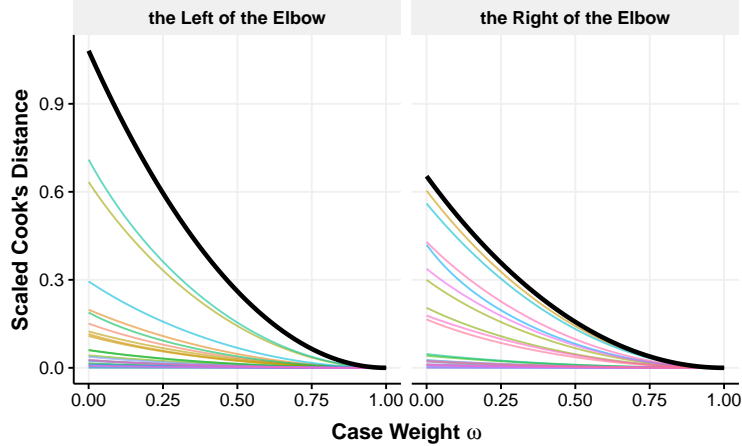


Figure 8: Case-influence graphs for ridge regression ($n = 50, p = 30$). The influence curves in the left and right panels correspond to cases with negative and positive full-data residuals, respectively. The bold curves correspond to the cases with the most positive or negative full-data residual.

illustration. The selected features are listed in Appendix A.7.1. These predictors describe the quality and characteristics of a house, including the square root of the living space in square footage, the presence of a basement, the number of bathrooms, and others.

In Subsection 5.1, we consider a quantile regression with a single predictor with a negligible fixed penalty. In Subsection 5.2, we utilize all 12 features for a multi-predictor quantile regression. In both subsections, the square root of the housing price is used as the response variable. A repository of the R code used in data analysis can be accessed at <https://github.com/hhzh-s/Case-Influence-in-Quantile-Regression>.

5.1 Quantile Regression with a Single Predictor

We consider a quantile regression with a single predictor for the ease of illustration. The square root of the average interior living room space in square footage from the closest 15 neighbors of a house is used as a predictor. For various quantiles $\tau = 0.1, 0.5$ and 0.95 , we set a negligible penalty of $\lambda = n * 0.01$ to obtain the case-weight adjusted solution path and the corresponding case-influence graph. This allows us to evaluate Cook's distance efficiently without refitting the model when one observation is excluded.

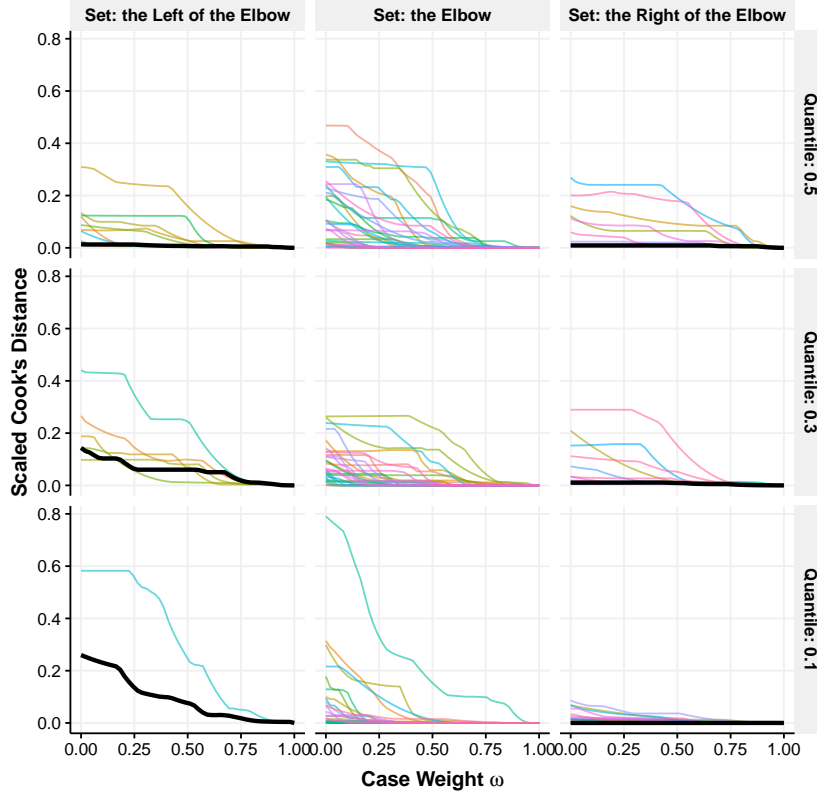


Figure 9: Case-influence graphs for penalized quantile regression with various quantiles ($\tau = 0.5, 0.3,$ and 0.1), $n = 50$ and $p = 30$. The left, middle and right panels correspond to cases with negative, zero and positive full-data residuals. The bold curves indicate the cases with the most positive or negative full-data residual.

Figure 10 illustrates how Cook's distance as a LOO influence measure is related to the relative extremeness of the predictor value and the residual in quantile regression. We observe that when $\tau = 0.1$, influential observations tend to have negative residuals. When $\tau = 0.5$, observations with either positive or negative residuals can exhibit a large influence. At $\tau = 0.95$, influential observations generally have positive residuals. In terms of the predictor, influential observations tend to have more extreme predictor values.

Figure 11 compares the fitted regression lines for different quantiles using the full data with those when each of the top 5 influential observations is removed. As shown in Figure 11, excluding the most influential observations from Figure 10 results in various changes to the fitted quantile regression lines, depending on the specific value of the quantile τ . The median regression appears to be the most robust, while the more extreme quantile

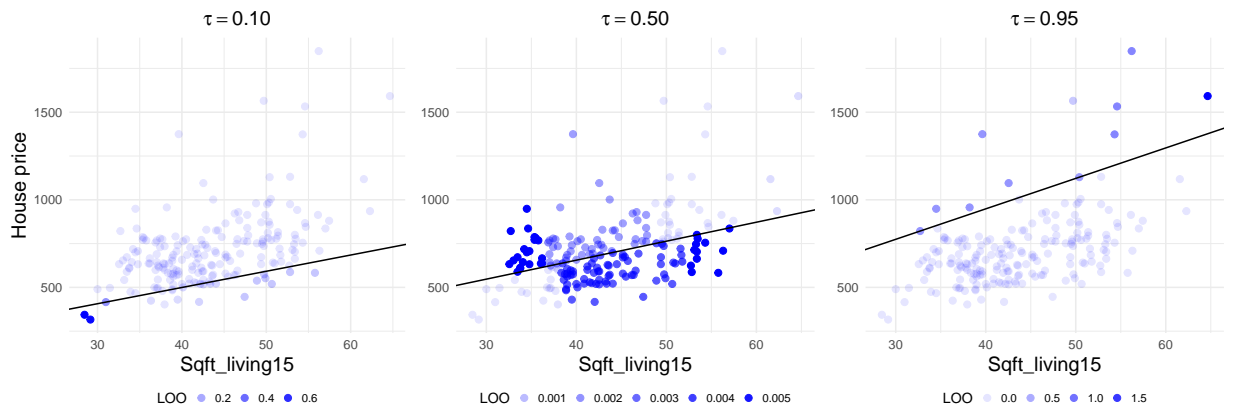


Figure 10: Scatter plot of house price versus the square root of the living room space in square footage from the nearest 15 neighbors for $\tau = 0.1$ (left), 0.5 (middle), and 0.95 (right). The solid black line in each panel represents the fitted quantile regression line. The shade of each point is determined by Cook's distance as a LOO influence measure and is defined separately for each quantile value.

regressions tend to be more sensitive to influential observations. This is also supported by a different magnitude of Cook's distance values across different quantiles in Figure 10.

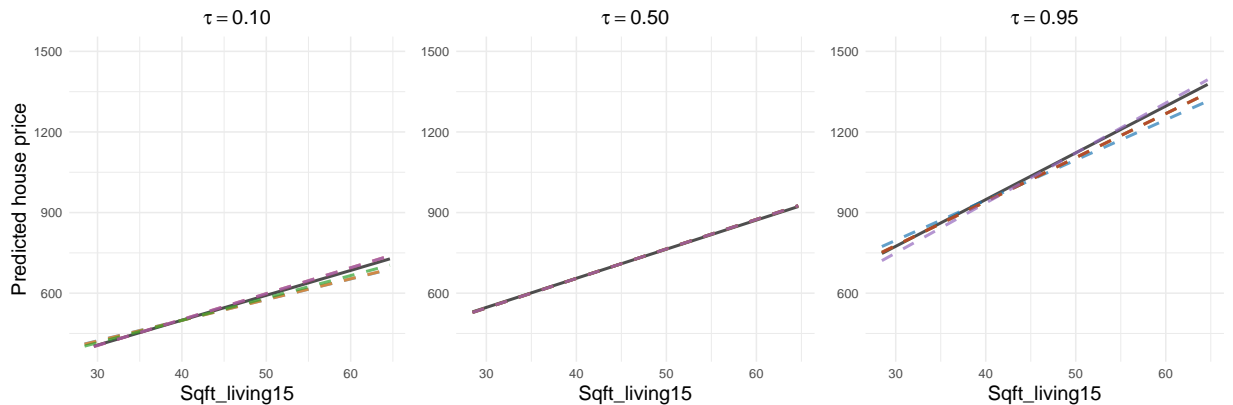


Figure 11: Fitted single-predictor quantile regression lines for the King County house sales data when $\tau = 0.1$ (left), 0.5 (middle), and 0.95 (right). The black solid lines are for the full-data solution, and the colored dashed lines are for the LOO solution when each of the top 5 influential observations is excluded.

Figure 15 in Appendix A.7.3 displays the case-influence graphs for each observation in the single-predictor quantile regression. As in Figure 10, when $\tau = 0.1$, the influence of the cases in the right elbow set remains consistently low across all $\omega \in [0, 1]$ while a couple of cases in the left elbow set have a relatively large influence. When $\tau = 0.5$, the case influence from the three sets is of the same scale. When $\tau = 0.95$, conversely, cases in the

right elbow set tend to be more influential.

The patterns of the case influence observed in Figures 10 and 15 can be explained through the property of the case-weight adjusted solution path. When adjusting the weight of a case (x_{i^*}, y_{i^*}) , the rate of change of the fitted value at x_i can be quantified as

$$\left. \frac{\partial \hat{f}_\omega(x_i)}{\partial \omega} \right|_{\omega=1} = \frac{1}{\lambda} \left[\frac{(q_0^\top \tilde{x}_i - 1)(q_0^\top \tilde{x}_{i^*} - 1)}{q_0^\top q_0} + \tilde{x}_i^\top (I - P_{\tilde{X}_{\mathcal{E}_0}}) \tilde{x}_{i^*} \right] \cdot (\tau - \mathbb{I}(i^* \in \mathcal{L}_0)), \quad (21)$$

where $q_0 = \tilde{X}_{\mathcal{E}_0}^\top (\tilde{X}_{\mathcal{E}_0} \tilde{X}_{\mathcal{E}_0}^\top)^{-1} \mathbf{1}_{\mathcal{E}_0} \in \mathbb{R}^{p+1}$ and $P_{\tilde{X}_{\mathcal{E}_0}} = \tilde{X}_{\mathcal{E}_0}^\top (\tilde{X}_{\mathcal{E}_0} \tilde{X}_{\mathcal{E}_0}^\top)^{-1} \tilde{X}_{\mathcal{E}_0}$ depend on the elbow set \mathcal{E}_0 . Details of the derivation of the result in (21) can be found in the proof of Proposition 1 in Tu (2019).

We refer to $(\tau - \mathbb{I}(i^* \in \mathcal{L}_0))$ as a generalized residual, which reflects the goodness-of-fit at (x_{i^*}, y_{i^*}) similarly to the usual residual $r_{i^*} = y_{i^*} - \hat{f}_{i^*}$. The generalized residual takes the value $\tau - 1$ when $r_{i^*} < 0$ and τ when $r_{i^*} > 0$. Therefore, when $\tau < 0.5$, influential observations tend to have negative residuals, as this leads to a larger generalized residual in the absolute value in quantile regression and implies more change in the fitted values when adjusting the weight of (x_{i^*}, y_{i^*}) .

In addition, the constant segments of the Cook's distance in Figure 15 are due to the property of the case-weight adjusted solution path when the elbow set is of full rank. Justification of this property is provided in Appendix A.7.3.

5.2 Quantile Regression with Multiple Predictors

To demonstrate how the computational and graphical tools for case influence assessment can be utilized in the presence of multiple predictors, we fit a multi-variable quantile regression using the 12 predictors. We selected the regularization parameter λ based on the empirical loss on a separate validation set of size 200. We may regard the term involving the predictor value in Equation (21) as the (i, i^*) entry of a generalized hat matrix akin to the hat matrix in least squares mean regression and refer to its diagonal entry as the

generalized leverage:

$$h_{i^*i^*} = \frac{1}{\lambda} \left[\frac{(q_0^\top \tilde{x}_{i^*} - 1)(q_0^\top \tilde{x}_{i^*} - 1)}{q_0^\top q_0} + \tilde{x}_{i^*}^\top (I - P_{\tilde{X}_{\varepsilon_0}}) \tilde{x}_{i^*} \right]. \quad (22)$$

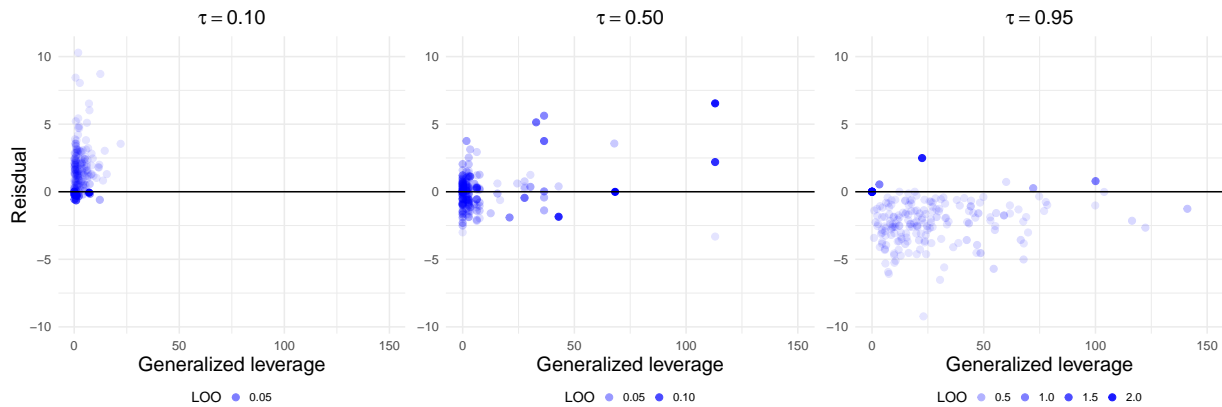


Figure 12: Scatter plot of the residual versus the generalized leverage when $\tau = 0.1$ (left), 0.5 (middle), and 0.95 (right). The shade of each point is determined by Cook’s distance as a LOO influence measure.

As illustrated in Figure 12, similar to how Cook’s distance in mean regression increases with leverage, case influence in quantile regression tends to be higher among observations with higher generalized leverage. However, the two types of leverage are distinct and may not align with each other, as generalized leverage depends on the quantile value τ through the elbow set. For instance, in Figure 12, the observation with the highest generalized leverage at $\tau = 0.95$ has a moderate value of generalized leverage at $\tau = 0.1$ unlike the leverage in least squares regression. We observe a similar pattern for the residuals as in the single-predictor quantile regression shown in Figure 10. Specifically, when $\tau < 0.5$, observations with negative residuals tend to be more influential, highlighting the importance of the residual sign in determining the influence in quantile regression.

Figure 13 shows the case-influence graphs for different quantile values based on the random sample of 200 houses. As illustrated in Figure 13, when $\tau = 0.1$, the houses in the left elbow set tend to be more influential than those in other sets. When $\tau = 0.5$, the three sets are similar in terms of the magnitude of the case influence. When $\tau = 0.95$, highly influential points tend to appear from the elbow set or right elbow set.

We compare the estimated coefficients from the full-data solution and the LOO solution when the observation with the largest Cook's distance is removed for each quantile level. Tables of the estimated coefficients are provided in Appendix A.7.4. As indicated in the tables, excluding the most influential observation could substantially change the quantile regression model, especially for extreme quantiles. For example, when $\tau = 0.95$, removing the most influential observation resulted in the reversal of statistical significance of multiple features.

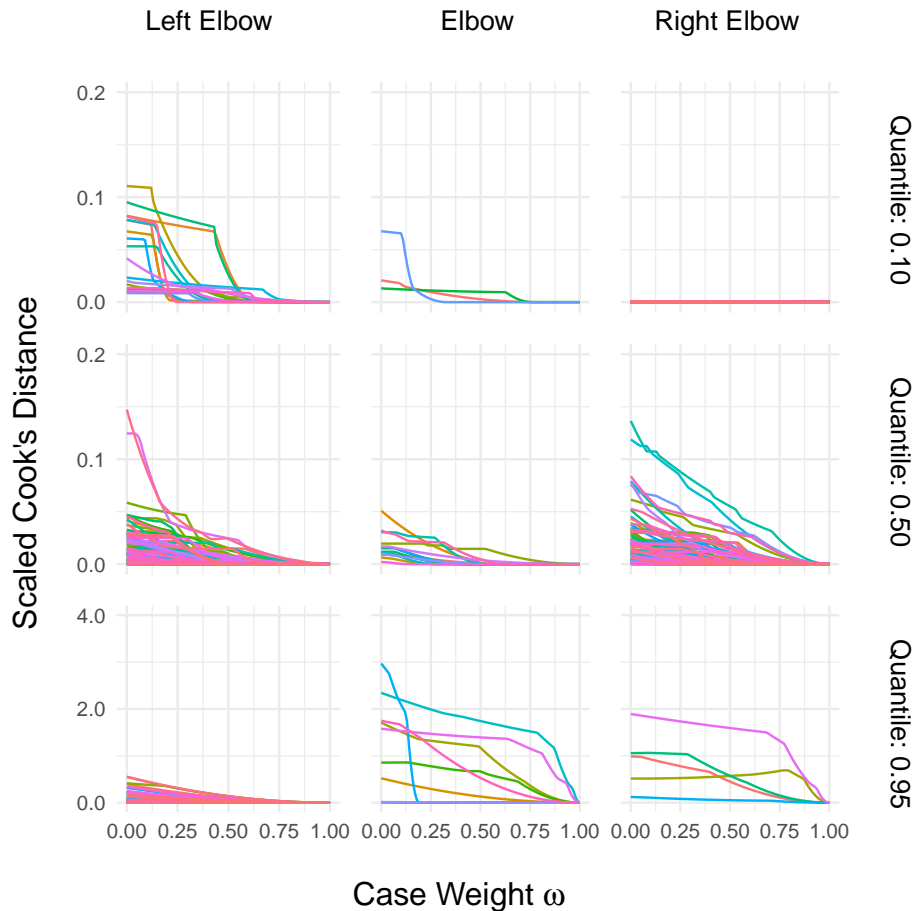


Figure 13: Case-influence graphs from an l_2 -penalized multi-predictor quantile regression for the King County house sales data with various quantiles: $\tau = 0.1$ (top), 0.5 (middle) and 0.95 (bottom). The left, middle and right panels correspond to the left elbow, elbow and right elbow set points, respectively.

6 Discussion

In this article, we have proposed a novel path-following algorithm to compute the leave-one-out cross validation scores exactly for quantile regression with ridge penalty. Numerical analysis has demonstrated that the proposed algorithm compares favorably to an alternative approach in terms of computational efficiency. Theoretically, we have provided a formal proof to establish the validity of the solution path algorithm. Moreover we have demonstrated that our proposed method can be used to efficiently compute the case-influence graph, which provides a more comprehensive approach to assessing case influence.

We have primarily focused on ℓ_2 penalized linear quantile regression. Similar case-weight adjusted path following algorithms can be derived for nonparametric quantile regression and ℓ_1 penalized quantile regression. Additionally, following the ideas proposed in [Rosset \(2009\)](#), it may be possible to derive a bi-level solution path for each pair of (λ, ω) , or even a tri-level path for each trio of (τ, λ, ω) . Furthermore, the idea of linking the full-data solution and the leave-one-out solution can be extended to classification settings. This will allow us to extend the notion of case influence to classification ([Koh and Liang, 2017](#)) and to study the stability of classifiers using case-influence measures. How to efficiently assess case influence in classification in itself is an important future direction.

Acknowledgements

This research was supported in part by National Science Foundation grants DMS-15-35666, DMS-17-21445, DMS-17-12580, and DMS-20-15490.

References

Allen, D. M. (1971). The prediction sum of squares as a criterion for selecting predictor variables, *Technical Report 23*, Department of Statistics, University of Kentucky.

- Allgower, E. and Georg, K. (1993). Continuation and path following, *Acta Numerica* **2**: 1 – 64.
- Belsley, D., Kuh, E. and Welsch, R. (1980). *Regression Diagnostics*, New York: Wiley.
- Chaouch, M. and Goga, C. (2010). Design-based estimation for geometric quantiles with application to outlier detection, *Computational Statistics and Data Analysis* **54**: 2214 – 2229.
- Cook, D. (1977). Detection of influential observations in linear regression, *Technometrics* **19**(1): 15 – 18.
- Cook, D. (1979). Influential observations in linear regression, *Journal of American Statistical Association* **74**(365): 169 – 174.
- Cook, D. (1986). Assessment of local influence, *Journal of the Royal Statistical Society. Series B (Methodological)* **48**(2): 133 – 169.
- Cook, D. and Weisberg, S. (1982). *Residuals and Influence in Regression*, Chapman and Hall.
- Craven, P. and Wahba, G. (1979). Smoothing noisy data with spline functions: Estimating the correct degree of smoothing by the method of generalized cross-validation, *Numerische Mathematik* **31**: 377 – 403.
- Efron, B., Hastie, T., Johnstone, I. and Tibshirani, R. (2004). Least angle regression, *The Annals of Statistics* **32**(2): 407 – 499.
- Hager, W. W. (1989). Updating the inverse of a matrix, *SIAM Review* **31**(2): 221 – 239.
- Hastie, T., Rosset, S., Tibshirani, R. and Zhu, J. (2004). The entire regularization path for the support vector machine, *Journal of Machine Learning Research* **5**: 1391 – 1415.
- Koenker, R. (2017). Quantile regression: 40 years on, *Annual Review of Economics* **9**: 155 – 176.

- Koenker, R. and Bassett, G. (1978). Regression quantiles, *Econometrica* **46**(1): 33 – 50.
- Koenker, R., Portnoy, S., Ng, P. T., Zeileis, A., Grosjean, P. and Ripley, B. D. (2018). Package ‘quantreg’, *Reference manual available at R-CRAN: <https://cran.rproject.org/web/packages/quantreg/quantreg.pdf>*.
- Koh, P. W. and Liang, P. (2017). Understanding black-box predictions via influence functions, *International Conference on Machine Learning*, PMLR, pp. 1885–1894.
- Kohavi, R. (1995). A study of cross-validation and bootstrap for accuracy estimation and model selection, *Proceedings of the 14th International Joint Conference on Artificial Intelligence (IJCAI)*, pp. 1137–1145.
- Li, Y., Liu, Y. and Zhu, J. (2007). Quantile regression in reproducing kernel Hilbert spaces, *Journal of American Statistical Association* **102**(477): 255 – 268.
- Li, Y. and Zhu, J. (2008). L_1 -norm quantile regression, *Journal of Computational and Graphical Statistics* **17**(1): 163 – 185.
- Luan, B., Lee, Y. and Zhu, Y. (2022). On measuring model complexity in heteroscedastic linear regression.
- Nychka, D., Gray, G., Haaland, P. and Martin, D. (1995). A nonparametric regression approach to syringe grading for quality improvement, *Journal of American Statistical Association* **90**(432): 1171 – 1178.
- Osborne, M. (1992). An effective method for computing regression quantiles, *IMA Journal of Numerical Analysis* **12**: 151 – 166.
- Osborne, M., Presnell, B. and Turlach, B. (2000). A new approach to variable selection in least squares problems, *IMA Journal of Numerical Analysis* **20**(3): 389 – 403.
- Reiss, P. and Huang, L. (2012). Smoothness selection for penalized quantile regression splines, *The International Journal of Biostatistics* **8**(1): Article 10.

- Rosset, S. (2009). Bi-level path following for cross validated solution of kernel quantile regression, *Journal of Machine Learning Research* **10**: 2473 – 2505.
- Rosset, S. and Zhu, J. (2007). Piecewise linear regularized solution paths, *The Annals of Statistics* **35**(3): 1012 – 1030.
- Stone, M. (1974). Cross-validatory choice and assessment of statistical predictions, *Journal of the Royal Statistical Society. Series B (Methodological)* **36**: 111 – 147.
- Takeuchi, I., Nomura, K. and Kanamori, T. (2009). Nonparametric conditional density estimation using piecewise-linear solution path of kernel quantile regression, *Neural Computation* **21**(2): 533 – 559.
- Tu, S. (2019). *Case Influence and Model Complexity in Regression and Classification*, Ph.d. dissertation, The Ohio State University, Columbus, OH.
- Wahba, G., Golub, G. and Health, M. (1979). Generalized cross-validation as a method for choosing a good ridge parameter, *Technometrics* pp. 215 – 223.
- Yuan, M. (2006). GACV for quantile smoothing splines, *Computational Statistics and Data Analysis* **50**: 813 – 829.
- Zhao, X., Zhang, S. and Liu, Q. (2012). Homotopy interior-point method for a general multiobjective programming problem, *Journal of Applied Mathematics* **77**: 1 – 12.

A Appendix

A.1 Derivation of KKT conditions (3)–(6)

We derive the KKT conditions for the optimization problem (2). Toward this end, let $(\beta_{0,\omega}, \beta_\omega)$ denote the solution of (2). By (1) and the fact that $\max(x, 0) = \inf_{t \geq 0, t \geq x} t$, we introduce auxiliary variables $\xi = (\xi_1, \dots, \xi_n)$ and $\zeta = (\zeta_1, \dots, \zeta_n)$ with $\xi_i \geq \max(y_i - \beta_0 - x_i^\top \beta, 0)$ and $\zeta_i \geq \max(-(y_i - \beta_0 - x_i^\top \beta), 0)$ for $i = 1, \dots, n$ to reexpress the check loss as follows:

$$\begin{aligned} \rho_\tau(y_i - \beta_0 - x_i^\top \beta) &= \tau \max(y_i - \beta_0 - x_i^\top \beta, 0) + (1 - \tau) \max(-(y_i - \beta_0 - x_i^\top \beta), 0) \\ &= \inf_{\xi_i, \zeta_i \geq 0 \text{ and } -\zeta_i \leq y_i - \beta_0 - x_i^\top \beta \leq \xi_i} \tau \xi_i + (1 - \tau) \zeta_i. \end{aligned}$$

Thus, we can rewrite the optimization problem (2) as

$$\begin{aligned} &\underset{\beta_0 \in \mathbb{R}, \beta \in \mathbb{R}^p, \xi \in \mathbb{R}^n, \zeta \in \mathbb{R}^n}{\text{minimize}} && \tau \sum_{i \neq i^*} \xi_i + (1 - \tau) \sum_{i \neq i^*} \zeta_i + \omega \tau \xi_{i^*} + \omega (1 - \tau) \zeta_{i^*} + \frac{\lambda}{2} \|\beta\|_2^2 \\ &\text{subject to} && -\zeta_i \leq y_i - \beta_0 - x_i^\top \beta \leq \xi_i, \text{ and } \zeta_i, \xi_i \geq 0 \text{ for } i = 1, \dots, n. \end{aligned} \quad (23)$$

Note that (23) is in the standard form of a constrained convex optimization problem:

$$\begin{aligned} &\underset{\mathbf{z} \in \mathbb{R}^\ell}{\text{minimize}} && f(\mathbf{z}) \\ &\text{subject to} && g_i(\mathbf{z}) \leq 0 \text{ for } i = 1, \dots, m, \end{aligned} \quad (24)$$

where $f(\cdot)$ and $g_i(\cdot)$ are convex functions. It is well-known that the KKT conditions for (24) are

$$\begin{aligned} \nabla f(\mathbf{z}) + \sum_{i=1}^m \lambda_i \nabla g_i(\mathbf{z}) &= 0, \text{ and} \\ \lambda_i g_i(\mathbf{z}) &= 0, \quad \text{for some real numbers } \lambda_i \geq 0, \quad i = 1, \dots, m. \end{aligned} \quad (25)$$

By letting $\mathbf{z} = (\beta_0, \beta, \xi, \zeta)$, $g_i(\mathbf{z}) = -\zeta_i$, $g_{n+i}(\mathbf{z}) = -\xi_i$, $g_{i+2n}(\mathbf{z}) = \beta_0 + x_i^\top \beta - y_i - \zeta_i$, and $g_{i+3n}(\mathbf{z}) = y_i - \beta_0 - x_i^\top \beta - \xi_i$ for $i = 1, \dots, n$, we next show that equations (3)–(6) are the KKT conditions for (23).

First, note that the Lagrangian function associated with (23) is

$$\begin{aligned}
L(\beta_0, \beta, \xi, \zeta, \alpha, \gamma, \kappa, \rho) &= \tau \sum_{i \neq i^*} \xi_i + (1 - \tau) \sum_{i \neq i^*} \zeta_i + \omega \tau \xi_{i^*} + \omega(1 - \tau) \zeta_{i^*} + \frac{\lambda}{2} \|\beta\|_2^2 \\
&+ \sum_{i=1}^n \alpha_i (y_i - \beta_0 - x_i^\top \beta - \xi_i) - \sum_{i=1}^n \gamma_i (y_i - \beta_0 - x_i^\top \beta + \zeta_i) - \sum_{i=1}^n \kappa_i \xi_i - \sum_{i=1}^n \rho_i \zeta_i,
\end{aligned}$$

where $\alpha_i, \gamma_i, \kappa_i, \rho_i \geq 0$ are the dual variables associated with the inequality constraints, and ξ_i and $\zeta_i \geq 0$ are primal variables introduced in (23). Hence, the Karush-Kuhn-Tucker (KKT) conditions are given by

$$\begin{aligned}
\frac{\partial L}{\partial \beta} &= \lambda \beta - \sum_{i=1}^n \alpha_i x_i + \sum_{i=1}^n \gamma_i x_i = 0, \\
\frac{\partial L}{\partial \beta_0} &= \sum_{i=1}^n (\alpha_i - \gamma_i) = 0, \\
\frac{\partial L}{\partial \xi_i} &= -\alpha_i - \kappa_i + \omega \tau + (1 - \omega) \tau \mathbf{1}_{\{i \neq i^*\}} = 0, \\
\frac{\partial L}{\partial \zeta_i} &= -\gamma_i - \rho_i + \omega(1 - \tau) + (1 - \omega)(1 - \tau) \mathbf{1}_{\{i \neq i^*\}} = 0, \\
\alpha_i (y_i - \beta_0 - x_i^\top \beta - \xi_i) &= 0, \quad \gamma_i (y_i - \beta_0 - x_i^\top \beta + \zeta_i) = 0, \quad \kappa_i \xi_i = 0, \quad \rho_i \zeta_i = 0, \\
-\zeta_i \leq y_i - \beta_0 - x_i^\top \beta \leq \xi_i, \quad \alpha_i \geq 0, \quad \gamma_i \geq 0, \quad \kappa_i \geq 0, \quad \rho_i \geq 0, \quad \xi_i \geq 0, \quad \zeta_i \geq 0, \quad i &= 1, \dots, n.
\end{aligned}$$

Defining $\theta_i := \alpha_i - \gamma_i$ for $i = 1, \dots, n$, we obtain (3) from the first two equations.

Note that when $y_i - \beta_0 - x_i^\top \beta > 0$, we must have $\xi_i \geq y_i - \beta_0 - x_i^\top \beta > 0$, which, together with $\kappa_i \xi_i = 0$, implies that $\kappa_i = 0$. Consequently, we have that $\alpha_i = \omega \tau + (1 - \omega) \tau \mathbb{I}_{\{i \neq i^*\}}$ and $\xi_i = y_i - \beta_0 - x_i^\top \beta$, because $\alpha_i \neq 0$. Moreover, we also have that $\gamma_i = 0$, because $\gamma_i (y_i - \beta_0 - x_i^\top \beta + \zeta_i) = 0$ and $\zeta_i \geq 0$. Hence, $\theta_i = \alpha_i - \gamma_i = \omega \tau + (1 - \omega) \tau \mathbb{I}_{\{i \neq i^*\}}$, which proves (6). Similarly, when $y_i - \beta_0 - x_i^\top \beta < 0$, we have that $\gamma_i = \omega(1 - \tau) + (1 - \omega)(1 - \tau) \mathbb{I}_{\{i \neq i^*\}}$ and $\alpha_i = 0$. Hence, $\theta_i = \alpha_i - \gamma_i = -\omega \tau - (1 - \omega) \tau \mathbb{I}_{\{i \neq i^*\}}$, which proves (4).

Finally, when $y_i - \beta_0 - x_i^\top \beta = 0$, we must have that $\xi_i = 0$, because $\alpha_i \xi_i = 0$, $\kappa_i \xi_i = 0$, and $\alpha_i + \kappa_i = \omega \tau + (1 - \omega) \tau \mathbb{I}_{\{i \neq i^*\}} > 0$. Similarly, $\zeta_i = 0$. Moreover, note that $\alpha_i \in [0, \omega \tau + (1 - \omega) \tau \mathbb{I}_{\{i \neq i^*\}}]$ and $\gamma_i \in [0, \omega(1 - \tau) + (1 - \omega)(1 - \tau) \mathbb{I}_{\{i \neq i^*\}}]$. Hence, $\theta_i = \alpha_i - \gamma_i \in$

$[-\omega(1 - \tau) - (1 - \omega)(1 - \tau)\mathbb{I}_{\{i \neq i^*\}}, \omega\tau + (1 - \omega)\tau\mathbb{I}_{\{i \neq i^*\}}]$, which proves (5).

A.2 Proof of Lemma 2

Lemma 2. *Let \mathcal{E}_m be the elbow set defined in Algorithm 1. Suppose that $\{(\tilde{x}_i, y_i)\}_{i=1}^n$ satisfies the general position condition that any $\min(p + 2, n)$ points of $\{(\tilde{x}_i, y_i)\}_{i=1}^n$ are linearly independent. Then we have $|\mathcal{E}_m| \leq p + 1$ and $\tilde{X}_{\mathcal{E}_m} \tilde{X}_{\mathcal{E}_m}^\top \succ 0$ for each $m = 0, 1, \dots, M$.*

Proof. We prove $\tilde{X}_{\mathcal{E}_m} \tilde{X}_{\mathcal{E}_m}^\top \succ 0$ by showing that (i) $|\mathcal{E}_m| \leq p + 1$ and (ii) the rows of $\tilde{X}_{\mathcal{E}_m}$ are linearly independent.

(i). We prove $|\mathcal{E}_m| \leq p + 1$ by contradiction. Suppose that $|\mathcal{E}_m| \geq p + 2$. Then we must have $p + 2 \leq |\mathcal{E}_m| \leq n$. Moreover, by the *general position condition*, we know that any $\min(n, p + 2) = p + 2$ points of $\{(\tilde{x}_i, y_i)\}_{i=1}^n$ are linearly independent, which implies that $\text{rank}(\tilde{X}_{\mathcal{E}_m}, Y_{\mathcal{E}_m}) \geq p + 2$. On the other hand, we can rewrite the KKT condition (5) as

$$y_{\mathcal{E}_m} = \beta_0 \mathbf{1}_{\mathcal{E}_m} + X_{\mathcal{E}_m} \beta = \tilde{X}_{\mathcal{E}_m} \begin{pmatrix} \beta_0 \\ \beta \end{pmatrix},$$

which implies that $\text{rank}(\tilde{X}_{\mathcal{E}_m}, Y_{\mathcal{E}_m}) = \text{rank}(\tilde{X}_{\mathcal{E}_m}) \leq \min(p + 1, n) \leq p + 1$. This is a contradiction. Thus $|\mathcal{E}_m| \leq p + 1$.

(ii). Since the number of rows of $\tilde{X}_{\mathcal{E}_m}$, $|\mathcal{E}_m| \leq \min(p + 1, n) \leq \min(p + 2, n)$ by (i), $\text{rank}(\tilde{X}_{\mathcal{E}_m}, Y_{\mathcal{E}_m}) = |\mathcal{E}_m|$ by the *general position condition*, which implies that $\text{rank}(\tilde{X}_{\mathcal{E}_m}) = |\mathcal{E}_m|$. Thus, the rows of $\tilde{X}_{\mathcal{E}_m}$ must be linearly independent. \square

A.3 Proof of Proposition 1

Since $\lambda r_\omega = \lambda(y - \beta_{0,\omega} \mathbf{1} - X\beta_\omega) = \lambda y - \lambda \beta_{0,\omega} \mathbf{1} - X X^\top \theta_\omega$, using the fact that $\lambda \beta_\omega = X^\top \theta_\omega$ from (3), we only need to derive the updating formulas for $\beta_{0,\omega}$ and $\theta_{\mathcal{E}_m,\omega}$.

Let $\tilde{X} = (\mathbf{1}, X)$ denote the expanded design matrix with each row $\tilde{x}_i^\top = (1, x_i^\top)$ for $i =$

$1, \dots, n$. Combining the first two equations in (7), we rewrite (7) as

$$\begin{aligned} \lambda \begin{pmatrix} 0 \\ \beta_\omega \end{pmatrix} - \tilde{X}_{\mathcal{E}_m}^\top \theta_{\mathcal{E}_m, \omega} &= \tilde{X}_{\mathcal{L}_m}^\top \theta_{\mathcal{L}_m, \omega} + \tilde{X}_{\mathcal{R}_m}^\top \theta_{\mathcal{R}_m, \omega}, \\ \beta_{0, \omega} \mathbf{1}_{\mathcal{E}_m} + \tilde{X}_{\mathcal{E}_m} \begin{pmatrix} 0 \\ \beta_\omega \end{pmatrix} &= y_{\mathcal{E}_m}. \end{aligned} \quad (26)$$

By eliminating β_ω from (26), we have that

$$(\tilde{X}_{\mathcal{E}_m} \tilde{X}_{\mathcal{E}_m}^\top) \theta_{\mathcal{E}_m, \omega} = [\lambda y_{\mathcal{E}_m} - \lambda \beta_{0, \omega} \mathbf{1}_{\mathcal{E}_m} - \tilde{X}_{\mathcal{E}_m} (\tilde{X}_{\mathcal{L}_m}^\top \theta_{\mathcal{L}_m, \omega} + \tilde{X}_{\mathcal{R}_m}^\top \theta_{\mathcal{R}_m, \omega})], \quad (27)$$

and

$$\mathbf{1}_{\mathcal{E}_m}^\top \theta_{\mathcal{E}_m, \omega} = -\mathbf{1}_{\mathcal{L}_m}^\top \theta_{\mathcal{L}_m, \omega} - \mathbf{1}_{\mathcal{R}_m}^\top \theta_{\mathcal{R}_m, \omega}. \quad (28)$$

Under the *general position condition*, we have that

$$\lambda \beta_{0, \omega} = \frac{\mathbf{1}_{\mathcal{E}_m}^\top (\tilde{X}_{\mathcal{E}_m} \tilde{X}_{\mathcal{E}_m}^\top)^{-1} (\lambda y_{\mathcal{E}_m} - \tilde{X}_{\mathcal{E}_m} (\tilde{X}_{\mathcal{L}_m}^\top \theta_{\mathcal{L}_m, \omega} + \tilde{X}_{\mathcal{R}_m}^\top \theta_{\mathcal{R}_m, \omega})) + \mathbf{1}_{\mathcal{L}_m}^\top \theta_{\mathcal{L}_m, \omega} + \mathbf{1}_{\mathcal{R}_m}^\top \theta_{\mathcal{R}_m, \omega}}{\mathbf{1}_{\mathcal{E}_m}^\top (\tilde{X}_{\mathcal{E}_m} \tilde{X}_{\mathcal{E}_m}^\top)^{-1} \mathbf{1}_{\mathcal{E}_m}} \quad (29)$$

and

$$\theta_{\mathcal{E}_m, \omega} = (\tilde{X}_{\mathcal{E}_m} \tilde{X}_{\mathcal{E}_m}^\top)^{-1} [\lambda y_{\mathcal{E}_m} - \lambda \beta_{0, \omega} \mathbf{1}_{\mathcal{E}_m} - \tilde{X}_{\mathcal{E}_m} (\tilde{X}_{\mathcal{L}_m}^\top \theta_{\mathcal{L}_m, \omega} + \tilde{X}_{\mathcal{R}_m}^\top \theta_{\mathcal{R}_m, \omega})], \quad (30)$$

where the fact that $\tilde{X}_{\mathcal{E}_m} \tilde{X}_{\mathcal{E}_m}^\top$ is invertible and $\mathbf{1}_{\mathcal{E}_m}^\top (\tilde{X}_{\mathcal{E}_m} \tilde{X}_{\mathcal{E}_m}^\top)^{-1} \mathbf{1}_{\mathcal{E}_m} \neq 0$ are ensured by the *general position condition* in view of Lemma 2.

From (29) and (30), note that the dependence of $\beta_{0, \omega}$ and $\theta_{\mathcal{E}_m, \omega}$ on ω stems from $\theta_{\mathcal{L}_m, \omega}$ and $\theta_{\mathcal{R}_m, \omega}$, which may be a function of ω depending on whether the weighted case i^* is in $\mathcal{L}_m \cup \mathcal{R}_m$ or not. More specifically, from (4)–(6), if case $i^* \in \mathcal{E}_m$, then $\beta_{0, \omega}$ and $\theta_{\mathcal{E}_m, \omega}$ are independent of ω , because $\theta_{\mathcal{L}_m, \omega}$ and $\theta_{\mathcal{R}_m, \omega}$ are both independent of ω . On the other hand, if case $i^* \in \mathcal{L}_m \cup \mathcal{R}_m$, then $\beta_{0, \omega}$ and $\theta_{\mathcal{E}_m, \omega}$ are linear in ω as $\theta_{i^*} = \omega(\tau - \mathbb{I}(i^* \in \mathcal{L}_m))$ is linear in ω . As a result, we consider these two cases separately to determine the next breakpoint:

- Case I: $i^* \in \mathcal{L}_m \cup \mathcal{R}_m$

- Case II: $i^* \in \mathcal{E}_m$

I. For Case I, note that

$$\theta_{i^*,\omega} = \omega[\tau - \mathbb{I}(i^* \in \mathcal{L}_m)] \text{ and } \theta_{i,\omega} = [\tau - \mathbb{I}(i \in \mathcal{L}_m)] \text{ for } i \neq i^* \text{ and } i \in \mathcal{L}_m \cup \mathcal{R}_m.$$

Hence, taking the difference of (29) at ω and ω_m , and using the fact that only $\theta_{i^*,\omega}$ changes with ω , we obtain that

$$\lambda\beta_{0,\omega} - \lambda\beta_{0,\omega_m} = b_{0,m}(\omega - \omega_m), \quad (31)$$

where

$$b_{0,m} = \frac{1 - \mathbf{1}_{\mathcal{E}_m}^\top (\tilde{X}_{\mathcal{E}_m} \tilde{X}_{\mathcal{E}_m}^\top)^{-1} \tilde{X}_{\mathcal{E}_m} \tilde{x}_{i^*}}{\mathbf{1}_{\mathcal{E}_m}^\top (\tilde{X}_{\mathcal{E}_m} \tilde{X}_{\mathcal{E}_m}^\top)^{-1} \mathbf{1}_{\mathcal{E}_m}} [\tau - \mathbb{I}(i^* \in \mathcal{L}_m)].$$

Similarly, taking the difference of (30) at ω and ω_m , we obtain that

$$\begin{aligned} & \theta_{\mathcal{E}_m,\omega} - \theta_{\mathcal{E}_m,\omega_m} \\ &= -(\tilde{X}_{\mathcal{E}_m} \tilde{X}_{\mathcal{E}_m}^\top)^{-1} \left[(\lambda\beta_{0,\omega} - \lambda\beta_{0,\omega_m}) \mathbf{1}_{\mathcal{E}_m} + \tilde{X}_{\mathcal{E}_m} \tilde{x}_{i^*} \{\tau - \mathbb{I}(i^* \in \mathcal{L}_m)\} (\omega - \omega_m) \right] \\ &= -(\tilde{X}_{\mathcal{E}_m} \tilde{X}_{\mathcal{E}_m}^\top)^{-1} \left[b_{0,m} \mathbf{1}_{\mathcal{E}_m} + \tilde{X}_{\mathcal{E}_m} \tilde{x}_{i^*} \{\tau - \mathbb{I}(i^* \in \mathcal{L}_m)\} \right] (\omega - \omega_m) \\ &= b_m(\omega - \omega_m), \end{aligned}$$

where

$$b_m = -(\tilde{X}_{\mathcal{E}_m} \tilde{X}_{\mathcal{E}_m}^\top)^{-1} \left[b_{0,m} \mathbf{1}_{\mathcal{E}_m} + \tilde{X}_{\mathcal{E}_m} \tilde{x}_{i^*} \{\tau - \mathbb{I}(i^* \in \mathcal{L}_m)\} \right].$$

This proves (8) and (9). Note that (8) and (9) give how $\theta_{\mathcal{E}_m,\omega}$ changes as a function of ω .

Next, we derive a similar formula for r_ω . To that end, multiplying both sides of the first equation in (26) by \tilde{X} , we have that for any $\omega \in [\omega_{m+1}, \omega_m]$,

$$\lambda \tilde{X} \begin{pmatrix} 0 \\ \beta_\omega \end{pmatrix} - \tilde{X} \tilde{X}_{\mathcal{E}_m}^\top \theta_{\mathcal{E}_m,\omega} = \tilde{X} \tilde{X}_{\mathcal{L}_m}^\top \theta_{\mathcal{L}_m,\omega} + \tilde{X} \tilde{X}_{\mathcal{R}_m}^\top \theta_{\mathcal{R}_m,\omega}.$$

Together with (4)–(6), this further implies that

$$\lambda \tilde{X} \begin{pmatrix} 0 \\ \beta_\omega - \beta_{\omega_m} \end{pmatrix} = \tilde{X} \tilde{X}_{\mathcal{E}_m}^\top (\theta_{\mathcal{E}_m, \omega} - \theta_{\mathcal{E}_m, \omega_m}) + \{\tau - \mathbb{I}(i^* \in \mathcal{L}_m)\} \tilde{X} \tilde{x}_{i^*} (\omega - \omega_m).$$

Combining this with (31) and (9), we obtain the following result for residual r_ω :

$$\begin{aligned} \lambda r_\omega - \lambda r_{\omega_m} &= \lambda \left(y - \tilde{X} \begin{pmatrix} \beta_{0, \omega} \\ \beta_\omega \end{pmatrix} \right) - \lambda \left(y - \tilde{X} \begin{pmatrix} \beta_{0, \omega_m} \\ \beta_{\omega_m} \end{pmatrix} \right) \\ &= -\lambda \tilde{X} \begin{pmatrix} 0 \\ \beta_\omega - \beta_{\omega_m} \end{pmatrix} - (\lambda \beta_{0, \omega} - \lambda \beta_{0, \omega_m}) \mathbf{1} \\ &= -\tilde{X} \tilde{X}_{\mathcal{E}_m}^\top (\theta_{\mathcal{E}_m, \omega} - \theta_{\mathcal{E}_m, \omega_m}) - \{\tau - \mathbb{I}(i^* \in \mathcal{L}_m)\} \tilde{X} \tilde{x}_{i^*} (\omega - \omega_m) - b_{0, m} (\omega - \omega_m) \mathbf{1} \\ &= -\tilde{X} \tilde{X}_{\mathcal{E}_m}^\top b_m (\omega - \omega_m) - \{\tau - \mathbb{I}(i^* \in \mathcal{L}_m)\} \tilde{X} \tilde{x}_{i^*} (\omega - \omega_m) - b_{0, m} (\omega - \omega_m) \mathbf{1} \\ &= h_m (\omega - \omega_m), \end{aligned}$$

where

$$h_m = -b_{0, m} \mathbf{1} - \tilde{X} \left[\tilde{X}_{\mathcal{E}_m}^\top b_m + \{\tau - \mathbb{I}(i^* \in \mathcal{L}_m)\} \tilde{x}_{i^*} \right].$$

This proves (11) and (12).

II. For Case II: $i^* \in \mathcal{E}_m$, we will show that $i^* \in \mathcal{E}_m$ can only happen when $m = 0$, and if that happens, i^* will move from \mathcal{E}_0 to $\mathcal{L}_1 \cup \mathcal{R}_1$ at the next breakpoint, and stay in $\mathcal{L}_m \cup \mathcal{R}_m$ for all $m = 1, \dots, M$. We show this by considering two scenarios.

- Scenario 1: if $i^* \in \mathcal{L}_0 \cup \mathcal{R}_0$, then case i^* will stay in $\mathcal{L}_m \cup \mathcal{R}_m$ for $m = 1, \dots, M$.
- Scenario 2: if $i^* \in \mathcal{E}_0$, then i^* will move from \mathcal{E}_0 to $\mathcal{L}_1 \cup \mathcal{R}_1$ at the next breakpoint, and stay in $\mathcal{L}_m \cup \mathcal{R}_m$ for $m = 1, \dots, M$.

For Scenario 1, we show that if $i^* \in \mathcal{L}_m \cup \mathcal{R}_m$, then case i^* will not move from $\mathcal{L}_m \cup \mathcal{R}_m$ to \mathcal{E}_m at the next breakpoint. We prove this by showing that the slope of the residual for case i^* over (ω_{m+1}, ω_m) is negative if $i^* \in \mathcal{R}_m$; and positive if $i^* \in \mathcal{L}_m$. Suppose that

$i^* \in \mathcal{R}_m$. In view of (11) and (12), we need to show that $\frac{\partial r_{i^*,\omega}}{\partial \omega} = h_{i^*,m} < 0$, or equivalently,

$$h_{i^*,m} = -b_{0,m} - \tilde{x}_{i^*}^\top \left[\tilde{X}_{\mathcal{E}_m}^\top b_m + \tilde{x}_{i^*} \tau \right] < 0. \quad (32)$$

By (9) and (10), we can show that

$$\begin{aligned} h_{i^*,m} &= - \left(b_{0,m} + \tilde{x}_{i^*}^\top \left[\tilde{X}_{\mathcal{E}_m}^\top b_m + \tilde{x}_{i^*} \tau \right] \right) \\ &= - \left(b_{0,m} - \tilde{x}_{i^*}^\top \left[\tilde{X}_{\mathcal{E}_m}^\top \left((\tilde{X}_{\mathcal{E}_m} \tilde{X}_{\mathcal{E}_m}^\top)^{-1} \left[b_{0,m} \mathbf{1}_{\mathcal{E}_m} + \tilde{X}_{\mathcal{E}_m} \tilde{x}_{i^*} \{ \tau - \mathbb{I}(i^* \in \mathcal{L}_m) \} \right] \right) + \tilde{x}_{i^*} \tau \right] \right) \\ &= - \left(b_{0,m} - \tilde{x}_{i^*}^\top \tilde{X}_{\mathcal{E}_m}^\top (\tilde{X}_{\mathcal{E}_m} \tilde{X}_{\mathcal{E}_m}^\top)^{-1} b_{0,m} \mathbf{1}_{\mathcal{E}_m} - \tilde{x}_{i^*}^\top \tilde{X}_{\mathcal{E}_m}^\top (\tilde{X}_{\mathcal{E}_m} \tilde{X}_{\mathcal{E}_m}^\top)^{-1} \tilde{X}_{\mathcal{E}_m} \tilde{x}_{i^*} \tau + \tilde{x}_{i^*}^\top \tilde{x}_{i^*} \tau \right) \\ &= -b_{0,m} \left(1 - \tilde{x}_{i^*}^\top \tilde{X}_{\mathcal{E}_m}^\top (\tilde{X}_{\mathcal{E}_m} \tilde{X}_{\mathcal{E}_m}^\top)^{-1} \mathbf{1}_{\mathcal{E}_m} \right) - \tau \tilde{x}_{i^*}^\top (I - \tilde{X}_{\mathcal{E}_m}^\top (\tilde{X}_{\mathcal{E}_m} \tilde{X}_{\mathcal{E}_m}^\top)^{-1} \tilde{X}_{\mathcal{E}_m}) \tilde{x}_{i^*} \\ &= -\tau \frac{(1 - \mathbf{1}_{\mathcal{E}_m}^\top (\tilde{X}_{\mathcal{E}_m} \tilde{X}_{\mathcal{E}_m}^\top)^{-1} \tilde{X}_{\mathcal{E}_m} \tilde{x}_{i^*})^2}{\mathbf{1}_{\mathcal{E}_m}^\top (\tilde{X}_{\mathcal{E}_m} \tilde{X}_{\mathcal{E}_m}^\top)^{-1} \mathbf{1}_{\mathcal{E}_m}} - \tau \tilde{x}_{i^*}^\top (I - \tilde{X}_{\mathcal{E}_m}^\top (\tilde{X}_{\mathcal{E}_m} \tilde{X}_{\mathcal{E}_m}^\top)^{-1} \tilde{X}_{\mathcal{E}_m}) \tilde{x}_{i^*} < 0, \end{aligned}$$

where the last inequality uses the fact that $\tilde{x}_{i^*}^\top (I - \tilde{X}_{\mathcal{E}_m}^\top (\tilde{X}_{\mathcal{E}_m} \tilde{X}_{\mathcal{E}_m}^\top)^{-1} \tilde{X}_{\mathcal{E}_m}) \tilde{x}_{i^*} > 0$ under the *general position condition*, which can be shown as follows. Note that the rows of $\tilde{X}_{\mathcal{E}_m}$ and \tilde{x}_i are linearly independent since $|\mathcal{E}_m \cup \{i\}| = |\mathcal{E}_{m-1}| \leq \min(n, p+1) \leq \min(n, p+2)$. Hence, $\tilde{x}_i^\top (I - \tilde{X}_{\mathcal{E}_m}^\top (\tilde{X}_{\mathcal{E}_m} \tilde{X}_{\mathcal{E}_m}^\top)^{-1} \tilde{X}_{\mathcal{E}_m}) \tilde{x}_i > 0$ since $\tilde{X}_{\mathcal{E}_m}^\top (\tilde{X}_{\mathcal{E}_m} \tilde{X}_{\mathcal{E}_m}^\top)^{-1} \tilde{X}_{\mathcal{E}_m}$ is the projection matrix for the row space of $\tilde{X}_{\mathcal{E}_m}$ and $\tilde{X}_{\mathcal{E}_m}^\top (\tilde{X}_{\mathcal{E}_m} \tilde{X}_{\mathcal{E}_m}^\top)^{-1} \tilde{X}_{\mathcal{E}_m} \tilde{x}_i \neq \tilde{x}_i$.

Similarly we can also show that when $i^* \in \mathcal{L}_m$,

$$\begin{aligned} h_{i^*,m} &= (1 - \tau) \frac{(1 - \mathbf{1}_{\mathcal{E}_m}^\top (\tilde{X}_{\mathcal{E}_m} \tilde{X}_{\mathcal{E}_m}^\top)^{-1} \tilde{X}_{\mathcal{E}_m} \tilde{x}_{i^*})^2}{\mathbf{1}_{\mathcal{E}_m}^\top (\tilde{X}_{\mathcal{E}_m} \tilde{X}_{\mathcal{E}_m}^\top)^{-1} \mathbf{1}_{\mathcal{E}_m}} + (1 - \tau) \tilde{x}_{i^*}^\top (I - \tilde{X}_{\mathcal{E}_m}^\top (\tilde{X}_{\mathcal{E}_m} \tilde{X}_{\mathcal{E}_m}^\top)^{-1} \tilde{X}_{\mathcal{E}_m}) \tilde{x}_{i^*} \\ &> 0. \end{aligned} \quad (33)$$

This finishes the proof for Scenario 1.

For Scenario 2, note that when $i^* \in \mathcal{E}_0$, all the residuals and θ_ω are constant as θ_ω and $(\beta_{0,\omega}, \beta_\omega)$ are independent of ω for $\omega \in [\omega_1, 1]$. As a result, the next breakpoint ω_1 can be

determined by setting $\theta_{i^*,\omega_0} = \omega\tau$ or $\omega(\tau - 1)$, that is,

$$\omega_1 = \begin{cases} \frac{\theta_{i^*,\omega_0}}{\tau} & \text{if } 0 < \theta_{i^*,\omega_0} < \tau \\ \frac{\theta_{i^*,\omega_0}}{\tau-1} & \text{if } \tau - 1 < \theta_{i^*,\omega_0} < 0, \text{ or } \omega_1 = \frac{\theta_{i^*,\omega_0}}{\tau - \mathbb{I}(\theta_{i^*,\omega_0} < 0)}, \\ 0 & \text{if } \theta_{i^*,\omega_0} = 0 \end{cases}, \quad (34)$$

and i^* will move from \mathcal{E}_0 to \mathcal{L}_1 or \mathcal{R}_1 at ω_1 . After ω_1 , by the same argument used for Scenario 1, we can show that i^* will stay in $\mathcal{L}_m \cup \mathcal{R}_m$ for $m = 1, \dots, M$. This proves Scenario 2.

In summary, $i^* \in \mathcal{E}_m$ can only happen when $m = 0$, and if that happens, i^* will move from \mathcal{E}_0 to \mathcal{L}_1 or \mathcal{R}_1 at the next breakpoint, and stay in $\mathcal{L}_m \cup \mathcal{R}_m$ for $m = 1, \dots, M$. This completes the proof of Proposition 1.

A.4 Algorithm 1

Algorithm 1: The ω Path Algorithm for Case-weight Adjusted Quantile Regression

```

1 Input:  $X \in \mathbb{R}^{n \times p}, y \in \mathbb{R}^n, \tau \in (0, 1), \lambda \in \mathbb{R}^+, i^* \in \{1, \dots, n\}, \hat{\beta}_{0, \omega_0}, \hat{\beta}_{\omega_0}$ 
2 Set  $\mathcal{L}_0 = \{i : y_i - \hat{\beta}_{0, \omega_0} - x_i^\top \hat{\beta}_{\omega_0} < 0\}, \mathcal{E}_0 = \{i : y_i - \hat{\beta}_{0, \omega_0} - x_i^\top \hat{\beta}_{\omega_0} = 0\},$ 
    $\mathcal{R}_0 = \{i : y_i - \hat{\beta}_{0, \omega_0} - x_i^\top \hat{\beta}_{\omega_0} > 0\}.$ 
3 Compute  $\hat{\theta}_{\omega_0}$  by setting  $\hat{\theta}_{\mathcal{L}_0, \omega_0} = (\tau - 1)\mathbf{1}, \hat{\theta}_{\mathcal{R}_0, \omega_0} = \tau\mathbf{1},$  and
    $\hat{\theta}_{\mathcal{E}_0, \omega_0} = (\tilde{X}_{\mathcal{E}_0} \tilde{X}_{\mathcal{E}_0}^\top)^{-1} [\lambda y_{\mathcal{E}_0} - \lambda \hat{\beta}_{0, \omega_0} \mathbf{1}_{\mathcal{E}_0} - \tilde{X}_{\mathcal{E}_0} (\tilde{X}_{\mathcal{L}_0}^\top \hat{\theta}_{\mathcal{L}_0, \omega_0} + \tilde{X}_{\mathcal{R}_0}^\top \hat{\theta}_{\mathcal{R}_0, \omega_0})]$  (see (30));
4 Set  $m = 0;$ 
5 if  $i^* \in \mathcal{E}_0$  then
6    $\omega_1 = \frac{\hat{\theta}_{i^*, \omega_0}}{\tau - \mathbb{I}(\hat{\theta}_{i^*, \omega_0} < 0)};$ 
7   Set  $(\hat{\beta}_\omega, \hat{\beta}_{0, \omega}, \hat{\theta}_\omega) = (\hat{\beta}_{\omega_0}, \hat{\beta}_{0, \omega_0}, \hat{\theta}_{\omega_0})$  for any  $\omega \in [\omega_1, 1];$ 
8   if  $\omega_1 > 0$  then
9     Update the three sets:  $(\mathcal{L}_1, \mathcal{E}_1, \mathcal{R}_1) = (\mathcal{L}_0, \mathcal{E}_0 \setminus \{i^*\}, \mathcal{R}_0 \cup \{i^*\})$  if  $\hat{\theta}_{i^*, \omega_0} > 0,$ 
10    otherwise  $(\mathcal{L}_1, \mathcal{E}_1, \mathcal{R}_1) = (\mathcal{L}_0 \cup \{i^*\}, \mathcal{E}_0 \setminus \{i^*\}, \mathcal{R}_0);$ 
11   end
12    $m = m + 1;$ 
13 end
14 while  $\omega_m > 0$  do
15   Compute the slopes  $(b_{0, m}, b_m, h_m)$  according to (10), (9) and (12), respectively;
16   Compute the next breakpoint  $\omega_{m+1}$  and its two candidates  $\omega_{1, m+1}$  and  $\omega_{2, m+1}$ 
   according to (13), (14a) and (14b);
17   For each  $\omega \in [\max(\omega_{m+1}, 0), \omega_m),$ 
   set
    $(\theta_{\mathcal{L}_m \setminus \{i^*\}, \omega}, \theta_{\mathcal{R}_m \setminus \{i^*\}, \omega}, \theta_{i^*, \omega}) = ((\tau - 1)\mathbf{1}_{\mathcal{L}_m \setminus \{i^*\}}, \tau \mathbf{1}_{\mathcal{R}_m \setminus \{i^*\}}, \omega(\tau - \mathbb{I}(i^* \in \mathcal{L}_m))),$ 
    $(\lambda \hat{\beta}_{0, \omega}, \hat{\theta}_{\mathcal{E}_m, \omega}) = (\lambda \hat{\beta}_{0, \omega_m}, \hat{\theta}_{\mathcal{E}_m, \omega_m}) + (b_{0, m}, b_m)(\omega - \omega_m)$  and
    $(\lambda \hat{\beta}_\omega, \lambda \hat{r}_\omega) = (\lambda \hat{\beta}_{\omega_m}, \lambda \hat{r}_{\omega_m}) + (X_{\mathcal{E}_m}^\top b_m + (\tau - \mathbb{I}(i^* \in \mathcal{L}_m))x_{i^*}, h_m)(\omega - \omega_m);$ 
18   Update the three sets:
19   if  $\omega_{m+1} = \omega_{1, m+1}$  then
20     Let  $i$  be the index that maximizes the objective function in (14a).
     Set  $(\mathcal{L}_{m+1}, \mathcal{E}_{m+1}, \mathcal{R}_{m+1}) = (\mathcal{L}_m, \mathcal{E}_m \setminus \{i\}, \mathcal{R}_m \cup \{i\})$  if  $\hat{\theta}_{i, \omega_{m+1}} = \tau,$  Rule
     (a)
21     otherwise  $(\mathcal{L}_{m+1}, \mathcal{E}_{m+1}, \mathcal{R}_{m+1}) = (\mathcal{L}_m \cup \{i\}, \mathcal{E}_m \setminus \{i\}, \mathcal{R}_m);$  Rule
     (b)
22   else
23     Let  $i$  be the index that maximizes the objective function in (14b).
     Set  $(\mathcal{L}_{m+1}, \mathcal{E}_{m+1}, \mathcal{R}_{m+1}) = (\mathcal{L}_m \setminus \{i\}, \mathcal{E}_m \cup \{i\}, \mathcal{R}_m)$  if  $i \in \mathcal{L}_m,$ 
24     otherwise  $(\mathcal{L}_{m+1}, \mathcal{E}_{m+1}, \mathcal{R}_{m+1}) = (\mathcal{L}_m, \mathcal{E}_m \cup \{i\}, \mathcal{R}_m \setminus \{i\});$  Rule
     (c)
25   end
26    $m = m + 1;$ 
27 end

```

A.5 Proof of Theorem 1

We only need to show that the case-weight adjusted path $(\hat{\beta}_{0,\omega}, \hat{\beta}_\omega, \hat{\theta}_\omega)$ generated by Algorithm 1 satisfies all the KKT conditions in (3)–(6). Our plan is to show that: (i) the initial full-data solution $(\hat{\beta}_{0,\omega_0}, \hat{\beta}_{\omega_0})$ together with $\hat{\theta}_{\omega_0}$ specified in Line 3 satisfies the KKT conditions at $\omega = \omega_0$; (ii) if $i^* \in \mathcal{E}_0$, then for each $\omega \in [\omega_1, 1]$, $(\hat{\beta}_{0,\omega}, \hat{\beta}_\omega, \hat{\theta}_\omega)$ in Line 7 satisfies the KKT conditions; and (iii) after Line 13 in Algorithm 1, $i^* \notin \mathcal{E}_m$ for each m , and $(\hat{\beta}_{0,\omega}, \hat{\beta}_\omega, \hat{\theta}_\omega)$ in Line 17 satisfies the KKT conditions.

(i) Note that $(\hat{\beta}_{0,\omega_0}, \hat{\beta}_{\omega_0})$ is the full-data solution. Thus, there must exist a vector $\theta \in \mathbb{R}^n$ such that $(\hat{\beta}_{0,\omega_0}, \hat{\beta}_{\omega_0}, \theta)$ satisfies the KKT conditions of (3)–(6). On the other hand, similar to the derivation of (30), we can show that θ must be unique and equal to $\hat{\theta}_{\omega_0}$ specified in Algorithm 1 given $(\hat{\beta}_{0,\omega_0}, \hat{\beta}_{\omega_0})$. Hence, $(\hat{\beta}_{0,\omega_0}, \hat{\beta}_{\omega_0}, \hat{\theta}_{\omega_0})$ satisfies the KKT conditions.

(ii) If the weighted case $i^* \in \mathcal{E}_0$, then for each $\omega \in [\omega_1, 1]$, $(\hat{\beta}_{0,\omega}, \hat{\beta}_\omega, \hat{\theta}_\omega) = (\hat{\beta}_{0,\omega_0}, \hat{\beta}_{\omega_0}, \hat{\theta}_{\omega_0})$, and thus it must also satisfy the KKT conditions (3)–(6), because the only condition in (3)–(6) that involves ω is $\theta_{i^*,\omega_0} \in [\omega(\tau - 1), \omega\tau]$, which remains to be true when $\omega \geq \omega_1 = \frac{\hat{\theta}_{i^*,\omega_0}}{\tau - \mathbb{I}(\hat{\theta}_{i^*,\omega_0} < 0)}$.

(iii) We use induction on m to show that $(\hat{\beta}_{0,\omega}, \hat{\beta}_\omega, \hat{\theta}_\omega)$ satisfies the KKT conditions for $\omega \in [\omega_{m+1}, \omega_m]$ and $i^* \notin \mathcal{E}_m$, after Line 13 of Algorithm 1. First we show that $i^* \notin \mathcal{E}_m$ after Line 13 of Algorithm 1. Using similar arguments in Part II of the proof of Proposition 1, we can show that if $i^* \in \mathcal{L}_m \cup \mathcal{R}_m$, then case i^* will not move from $\mathcal{L}_m \cup \mathcal{R}_m$ to \mathcal{E}_m at the next breakpoint. This can be verified using (32) and (33), both of which are still valid here since $b_{0,m}$ and b_m in Line 15 are computed according to (9) and (10) in Proposition 1. Hence, we must have $i^* \in \mathcal{L}_m \cup \mathcal{R}_m$ after Line 13 of Algorithm 1.

Next, we show that $(\hat{\beta}_{0,\omega}, \hat{\beta}_\omega, \hat{\theta}_\omega)$ satisfies the KKT conditions for $\omega \in [\omega_{m+1}, \omega_m]$ after Line 13 of Algorithm 1, provided that $i^* \notin \mathcal{E}_m$. In other words, we show that for each $\omega \in [\omega_{m+1}, \omega_m]$, $(\hat{\beta}_{0,\omega}, \hat{\beta}_\omega, \hat{\theta}_\omega)$ generated by Algorithm 1 satisfies the KKT conditions provided that $(\hat{\beta}_{0,\omega_m}, \hat{\beta}_{\omega_m}, \hat{\theta}_{\omega_m})$ satisfies the KKT conditions at breakpoint ω_m . Note that the KKT conditions consist of equality conditions and inequality conditions. We verify them separately.

Equality conditions: First, we verify that the following equality conditions are satisfied between breakpoints ω_m and ω_{m+1} :

$$\begin{aligned} \hat{\theta}_{\mathcal{L}_m \setminus \{i^*\}, \omega} &= (\tau - 1)1_{\mathcal{L}_m \setminus \{i^*\}}, & \hat{\theta}_{\mathcal{R}_m \setminus \{i^*\}, \omega} &= \tau 1_{\mathcal{R}_m \setminus \{i^*\}}, & \hat{\theta}_{i^*, \omega} &= \omega(\tau - \mathbb{I}(i^* \in \mathcal{L}_m)) \\ \tilde{X}^\top \hat{\theta}_\omega &= \begin{pmatrix} 0 \\ \lambda \hat{\beta}_\omega \end{pmatrix}, & \tilde{X}_{\mathcal{E}_m} \begin{pmatrix} \hat{\beta}_{0,m} \\ \hat{\beta}_m \end{pmatrix} &= y_{\mathcal{E}_m}. \end{aligned} \quad (35)$$

Since the above equality conditions are satisfied at $\omega = \omega_m$, it is sufficient to show that for each $\omega \in [\omega_{m+1}, \omega_m]$,

$$\begin{cases} \tilde{X}^\top (\hat{\theta}_\omega - \hat{\theta}_{\omega_m}) = \begin{pmatrix} 0 \\ \lambda(\hat{\beta}_\omega - \hat{\beta}_{\omega_m}) \end{pmatrix} \\ \tilde{X}_{\mathcal{E}_m} \begin{pmatrix} \hat{\beta}_{0,\omega} - \hat{\beta}_{0,\omega_m} \\ \hat{\beta}_\omega - \hat{\beta}_{\omega_m} \end{pmatrix} = \mathbf{0}. \end{cases} \quad (36a)$$

$$\tilde{X}_{\mathcal{E}_m} \begin{pmatrix} \hat{\beta}_{0,\omega} - \hat{\beta}_{0,\omega_m} \\ \hat{\beta}_\omega - \hat{\beta}_{\omega_m} \end{pmatrix} = \mathbf{0}. \quad (36b)$$

To prove (36a), first we see that

$$\begin{aligned} \tilde{X}^\top (\hat{\theta}_\omega - \hat{\theta}_{\omega_m}) &= \tilde{X}_{\mathcal{L}_m}^\top (\hat{\theta}_{\mathcal{L}_m, \omega} - \hat{\theta}_{\mathcal{L}_m, \omega_m}) + \tilde{X}_{\mathcal{R}_m}^\top (\hat{\theta}_{\mathcal{R}_m, \omega} - \hat{\theta}_{\mathcal{R}_m, \omega_m}) + \tilde{X}_{\mathcal{E}_m}^\top (\hat{\theta}_{\mathcal{E}_m, \omega} - \hat{\theta}_{\mathcal{E}_m, \omega_m}) \\ &= \{\tau - \mathbb{I}(i^* \in \mathcal{L}_m)\} \tilde{x}_{i^*} (\omega - \omega_m) + \tilde{X}_{\mathcal{E}_m}^\top b_m (\omega - \omega_m) \quad \text{by (9)} \\ &= \left(\{\tau - \mathbb{I}(i^* \in \mathcal{L}_m)\} \tilde{x}_{i^*} + \tilde{X}_{\mathcal{E}_m}^\top b_m \right) (\omega - \omega_m) \\ &= \begin{pmatrix} (\{\tau - \mathbb{I}(i^* \in \mathcal{L}_m)\} + 1_{\mathcal{E}_m}^\top b_m) (\omega - \omega_m) \\ (\{\tau - \mathbb{I}(i^* \in \mathcal{L}_m)\} x_{i^*} + X_{\mathcal{E}_m}^\top b_m) (\omega - \omega_m) \end{pmatrix}. \end{aligned}$$

Moreover, by (9) and (10), we can show that

$$\begin{aligned} -1_{\mathcal{E}_m}^\top b_m &= 1_{\mathcal{E}_m}^\top (\tilde{X}_{\mathcal{E}_m} \tilde{X}_{\mathcal{E}_m}^\top)^{-1} \left[b_{0,m} 1_{\mathcal{E}_m} + \tilde{X}_{\mathcal{E}_m} \tilde{x}_{i^*} \{\tau - \mathbb{I}(i^* \in \mathcal{L}_m)\} \right] \\ &= b_{0,m} 1_{\mathcal{E}_m}^\top (\tilde{X}_{\mathcal{E}_m} \tilde{X}_{\mathcal{E}_m}^\top)^{-1} 1_{\mathcal{E}_m} + 1_{\mathcal{E}_m}^\top (\tilde{X}_{\mathcal{E}_m} \tilde{X}_{\mathcal{E}_m}^\top)^{-1} \tilde{X}_{\mathcal{E}_m} \tilde{x}_{i^*} \{\tau - \mathbb{I}(i^* \in \mathcal{L}_m)\} \\ &= \left(1 - 1_{\mathcal{E}_m}^\top (\tilde{X}_{\mathcal{E}_m} \tilde{X}_{\mathcal{E}_m}^\top)^{-1} \tilde{X}_{\mathcal{E}_m} \tilde{x}_{i^*} \right) \{\tau - \mathbb{I}(i^* \in \mathcal{L}_m)\} + 1_{\mathcal{E}_m}^\top (\tilde{X}_{\mathcal{E}_m} \tilde{X}_{\mathcal{E}_m}^\top)^{-1} \tilde{X}_{\mathcal{E}_m} \tilde{x}_{i^*} \{\tau - \mathbb{I}(i^* \in \mathcal{L}_m)\} \\ &= \tau - \mathbb{I}(i^* \in \mathcal{L}_m). \end{aligned}$$

Combining this with Line 17 of Algorithm 1, we obtain (36a).

To prove (36b), by (36a), (31), (8), and (9), it follows that

$$\begin{aligned}
\lambda \tilde{X}_{\mathcal{E}_m} \begin{pmatrix} \hat{\beta}_{0,\omega} - \hat{\beta}_{0,\omega_m} \\ \hat{\beta}_\omega - \hat{\beta}_{\omega_m} \end{pmatrix} &= \tilde{X}_{\mathcal{E}_m} \begin{pmatrix} \lambda(\hat{\beta}_{0,\omega} - \hat{\beta}_{0,\omega_m}) \\ \mathbf{0} \end{pmatrix} + \tilde{X}_{\mathcal{E}_m} \begin{pmatrix} 0 \\ \lambda(\hat{\beta}_\omega - \hat{\beta}_{\omega_m}) \end{pmatrix} \\
&= \lambda(\hat{\beta}_{0,\omega} - \hat{\beta}_{0,\omega_m}) \mathbf{1}_{\mathcal{E}_m} + \tilde{X}_{\mathcal{E}_m} \tilde{X}_{\mathcal{E}_m}^\top (\hat{\theta}_\omega - \hat{\theta}_{\omega_m}) \\
&= \left(b_{0,m} \mathbf{1}_{\mathcal{E}_m} + \tilde{X}_{\mathcal{E}_m} \tilde{X}_{\mathcal{E}_m}^\top b_m + \tilde{X}_{\mathcal{E}_m} \tilde{x}_{i^*} \{\tau - \mathbb{I}(i^* \in \mathcal{L}_m)\} \right) (\omega - \omega_m) \\
&= \left(b_{0,m} \mathbf{1}_{\mathcal{E}_m} + \tilde{X}_{\mathcal{E}_m} \tilde{x}_{i^*} \{\tau - \mathbb{I}(i^* \in \mathcal{L}_m)\} - \right. \\
&\quad \left. \tilde{X}_{\mathcal{E}_m} \tilde{X}_{\mathcal{E}_m}^\top (\tilde{X}_{\mathcal{E}_m} \tilde{X}_{\mathcal{E}_m}^\top)^{-1} \left[b_{0,m} \mathbf{1}_{\mathcal{E}_m} + \tilde{X}_{\mathcal{E}_m} \tilde{x}_{i^*} \{\tau - \mathbb{I}(i^* \in \mathcal{L}_m)\} \right] \right) (\omega - \omega_m) \\
&= 0.
\end{aligned}$$

Inequality conditions: Next we verify the inequality conditions between breakpoints ω_m and ω_{m+1} . For this, we consider two cases: $m = \mathbb{I}(i^* \in \mathcal{E}_0)$ and $m \geq \mathbb{I}(i^* \in \mathcal{E}_0) + 1$. In the first case, if $i^* \notin \mathcal{E}_0$, then $m = 0$, and all inequality conditions are trivially satisfied for $\omega \in [\omega_1, 1]$. If $i^* \in \mathcal{E}_0$, then $m = 1$. Now for $\omega \in [\omega_2, \omega_1]$, we need to verify that $r_{i^*,\omega} > 0$ if $i^* \in \mathcal{R}_1$, and $r_{i^*,\omega} < 0$ if $i^* \in \mathcal{L}_1$. In fact, by similar arguments used in the proof of Part II of Proposition 1, it can be shown that the residual of case i^* will increase if $i^* \in \mathcal{R}_1$ and will decrease if $i^* \in \mathcal{L}_1$. Moreover, since $i^* \in \mathcal{E}_0$, we must have $r_{i^*,\omega_1} = 0$. Combining, we have that that $r_{i^*,\omega} > 0$ if $i^* \in \mathcal{R}_1$ and $r_{i^*,\omega} < 0$ if $i^* \in \mathcal{L}_1$.

In the second case of $m \geq \mathbb{I}(i^* \in \mathcal{E}_0) + 1$, we have that $i^* \notin \mathcal{E}_m$ and $i^* \notin \mathcal{E}_{m-1}$ since $i^* \notin \mathcal{E}_m$ after Line 13. In addition, as we have shown before, the sign of the residual of case i^* does not change after Line 13. Under these conditions, we next show that all the inequality conditions are satisfied by verifying that the three rules in Algorithm 1 to update the elbow set and non-elbow sets at each breakpoint are consistent with the signs of resulting residuals. Specifically, we need to verify that, for rule (a), if $\hat{\theta}_{i,\omega_m} = \tau$ for some $i \in \mathcal{E}_{m-1}$, then $r_{i,\omega} > 0$ for $\omega \in (\omega_{m+1}, \omega_m)$; for rule (b), if $\hat{\theta}_{i,\omega_m} = \tau - 1$ for some $i \in \mathcal{E}_{m-1}$, then $r_{i,\omega} < 0$ for $\omega \in (\omega_{m+1}, \omega_m)$, and for rule (c), if $r_{i,\omega_m} = 0$ for some $i \in \mathcal{L}_{m-1} \cup \mathcal{R}_{m-1}$,

then $\theta_{i,\omega} \in (\tau - 1, \tau)$ for $\omega \in (\omega_{m+1}, \omega_m)$.

For rule (a), if there exists $i \in \mathcal{E}_{m-1}$ such that $\hat{\theta}_{i,\omega_m} = \tau$ at ω_m , the rule sets $\mathcal{E}_m = \mathcal{E}_{m-1} \setminus \{i\}$ and $\mathcal{R}_m = \mathcal{R}_{m-1} \cup \{i\}$. We need to show that $r_{i,\omega} > 0$ for $\omega \in (\omega_{m+1}, \omega_m)$. Since $r_{i,\omega_m} = 0$, we need to show that $h_{i,m}$ —the slope of $r_{i,\omega}$ —is negative. In view of (12) and the fact that $\mathcal{E}_m = \mathcal{E}_{m-1} \setminus \{i\}$, we need to prove that

$$-h_{i,m} = b_{0,m} + \tilde{x}_i^\top [\tilde{X}_{\mathcal{E}_{m-1} \setminus \{i\}}^\top b_m + \tilde{x}_{i^*}(\tau - \mathbb{I}(i^* \in \mathcal{L}_m))] > 0. \quad (37)$$

Since $i \in \mathcal{E}_{m-1}$, we have that $\lambda r_{i,\omega} \equiv 0$ for $\omega \in (\omega_m, \omega_{m-1}]$, which implies that its slope $h_{i,m-1} = 0$. This, together with (12), implies that

$$\begin{aligned} -h_{i,m-1} &= b_{0,m-1} + \tilde{x}_i^\top [\tilde{X}_{\mathcal{E}_{m-1}}^\top b_{m-1} + \tilde{x}_{i^*}(\tau - \mathbb{I}(i^* \in \mathcal{L}_{m-1}))] \\ &= b_{0,m-1} + \tilde{x}_i^\top [\tilde{X}_{\mathcal{E}_m}^\top b_{\mathcal{E}_m, m-1} + \tilde{x}_i b_{i,m-1} + \tilde{x}_{i^*}(\tau - \mathbb{I}(i^* \in \mathcal{L}_{m-1}))] = 0. \end{aligned} \quad (38)$$

Moreover, note that $\mathbb{I}(i^* \in \mathcal{L}_{m-1}) = \mathbb{I}(i^* \in \mathcal{L}_m)$ for $m \geq 1 + \mathbb{I}(i^* \in \mathcal{E}_0)$ since $i^* \notin \mathcal{E}_m$ and $i \neq i^*$. In view of (38), (37) is equivalent to

$$b_{0,m} + \tilde{x}_i^\top \tilde{X}_{\mathcal{E}_{m-1} \setminus \{i\}}^\top b_m > b_{0,m-1} + \tilde{x}_i^\top \tilde{X}_{\mathcal{E}_{m-1} \setminus \{i\}}^\top b_{\mathcal{E}_{m-1} \setminus \{i\}, m-1} + \tilde{x}_i^\top \tilde{x}_i b_{i,m-1},$$

or

$$(b_{0,m} - b_{0,m-1}) + \tilde{x}_i^\top \tilde{X}_{\mathcal{E}_m}^\top (b_m - b_{\mathcal{E}_m, m-1}) - \tilde{x}_i^\top \tilde{x}_i b_{i,m-1} > 0. \quad (39)$$

Next we plan to show that

$$\begin{aligned} &(b_m - b_{\mathcal{E}_m, m-1}) - \tilde{x}_i^\top \tilde{x}_i b_{i,m-1} \\ &= b_{i,m-1} \left(-\frac{(1_{\mathcal{E}_m}^\top (\tilde{X}_{\mathcal{E}_m} \tilde{X}_{\mathcal{E}_m}^\top)^{-1} \tilde{X}_{\mathcal{E}_m} \tilde{x}_i - 1)^2}{1_{\mathcal{E}_m}^\top (\tilde{X}_{\mathcal{E}_m} \tilde{X}_{\mathcal{E}_m}^\top)^{-1} 1_{\mathcal{E}_m}} - \tilde{x}_i^\top (I - \tilde{X}_{\mathcal{E}_m}^\top (\tilde{X}_{\mathcal{E}_m} \tilde{X}_{\mathcal{E}_m}^\top)^{-1} \tilde{X}_{\mathcal{E}_m}) \tilde{x}_i \right) \end{aligned} \quad (40)$$

To that end, from the second equation in (35), we know that $1^\top \hat{\theta}_\omega = 0$ for $\omega \in (\omega_{m+1}, \omega_m]$.

Hence, for any $\omega \in (\omega_{m+1}, \omega_m)$,

$$\begin{aligned} 1_{\mathcal{E}_m}^\top \hat{\theta}_{\mathcal{E}_m, \omega} + 1_{\mathcal{L}_m}^\top \hat{\theta}_{\mathcal{L}_m, \omega} + 1_{\mathcal{R}_m}^\top \hat{\theta}_{\mathcal{R}_m, \omega} &= 0 \\ 1_{\mathcal{E}_m}^\top \hat{\theta}_{\mathcal{E}_m, \omega_m} + 1_{\mathcal{L}_m}^\top \hat{\theta}_{\mathcal{L}_m, \omega_m} + 1_{\mathcal{R}_m}^\top \hat{\theta}_{\mathcal{R}_m, \omega_m} &= 0 \end{aligned} \quad (41)$$

Taking difference of the above two equations and using the updating formula for $\hat{\theta}_{\mathcal{E}_m, \omega}$, we obtain that

$$1_{\mathcal{E}_m}^\top b_m (\omega - \omega_m) + (\tau - \mathbb{I}(i^* \in \mathcal{L}_m)) (\omega - \omega_m) = 0. \quad (42)$$

Dividing both sides by $\omega - \omega_m$, (42) reduces to

$$1_{\mathcal{E}_m}^\top b_m + (\tau - \mathbb{I}(i^* \in \mathcal{L}_m)) = 0.$$

Similarly, we also have that

$$1_{\mathcal{E}_{m-1}}^\top b_{m-1} + (\tau - \mathbb{I}(i^* \in \mathcal{L}_{m-1})) = 0.$$

Taking the difference and using the fact that $\mathbb{I}(i^* \in \mathcal{L}_{m-1}) = \mathbb{I}(i^* \in \mathcal{L}_m)$ for $m \geq 1 + \mathbb{I}(i^* \in \mathcal{E}_0)$, we obtain that

$$b_{i, m-1} = 1_{\mathcal{E}_m}^\top b_m - 1_{\mathcal{E}_m}^\top b_{\mathcal{E}_m, m-1} := 1_{\mathcal{E}_m}^\top \Delta_{\mathcal{E}_m}, \quad (43)$$

where $\Delta_{\mathcal{E}_m} = b_m - b_{\mathcal{E}_m, m-1}$. On the other hand, for any $j \in \mathcal{E}_m$, $r_{j, m-1} = r_{j, m} = 0$ implies their slopes $h_{j, m-1} = h_{j, m} = 0$. Hence, we have that $h_{\mathcal{E}_{m-1} \setminus \{i\}, m-1} = 0$ and $h_{\mathcal{E}_{m-1} \setminus \{i\}, m} = 0$, which implies that

$$\begin{aligned} b_{0, m-1} 1_{\mathcal{E}_m} + \tilde{X}_{\mathcal{E}_m} [\tilde{X}_{\mathcal{E}_m}^\top b_{\mathcal{E}_m, m-1} + b_{i, m-1} \tilde{x}_i + \tilde{x}_{i^*} (\tau - \mathbb{I}(i^* \in \mathcal{L}_{m-1}))] &= 0, \\ b_{0, m} 1_{\mathcal{E}_m} + \tilde{X}_{\mathcal{E}_m} [\tilde{X}_{\mathcal{E}_m}^\top b_m + \tilde{x}_{i^*} (\tau - \mathbb{I}(i^* \in \mathcal{L}_m))] &= 0. \end{aligned}$$

Again, because of $\mathbb{I}(i^* \in \mathcal{L}_{m-1}) = \mathbb{I}(i^* \in \mathcal{L}_m)$ for $m \geq 1 + \mathbb{I}(i^* \in \mathcal{E}_0)$, taking the difference, we obtain that

$$\Delta_0 1_{\mathcal{E}_m} + \tilde{X}_{\mathcal{E}_m} \tilde{X}_{\mathcal{E}_m}^\top \Delta_{\mathcal{E}_m} - \tilde{X}_{\mathcal{E}_m} \tilde{x}_i b_{i, m-1} = 0, \quad (44)$$

where $\Delta_0 = b_{0,m} - b_{0,m-1}$. Combining (43) and (44) and solving for $\Delta_{\mathcal{E}_m}$ and Δ_0 , we obtain that

$$\begin{aligned}\Delta_{\mathcal{E}_m} &= (\tilde{X}_{\mathcal{E}_m} \tilde{X}_{\mathcal{E}_m}^\top)^{-1} (\tilde{X}_{\mathcal{E}_m} \tilde{x}_i b_{i,m-1} - \Delta_0 \mathbf{1}_{\mathcal{E}_m}), \\ \Delta_0 &= \frac{(\mathbf{1}_{\mathcal{E}_m}^\top (\tilde{X}_{\mathcal{E}_m} \tilde{X}_{\mathcal{E}_m}^\top)^{-1} \tilde{X}_{\mathcal{E}_m} \tilde{x}_i - 1) b_{i,m-1}}{\mathbf{1}_{\mathcal{E}_m}^\top (\tilde{X}_{\mathcal{E}_m} \tilde{X}_{\mathcal{E}_m}^\top)^{-1} \mathbf{1}_{\mathcal{E}_m}}.\end{aligned}$$

Substituting the above into the LHS of (39), we have that

$$\begin{aligned}\text{LHS of (39)} &= (b_{0,m} - b_{0,m-1}) + \tilde{x}_i^\top \tilde{X}_{\mathcal{E}_m}^\top (b_m - b_{\mathcal{E}_m, m-1}) - \tilde{x}_i^\top \tilde{x}_i b_{i,m-1} = \Delta_0 + \tilde{x}_i^\top \tilde{X}_{\mathcal{E}_m}^\top \Delta_{\mathcal{E}_m} - \tilde{x}_i^\top \tilde{x}_i b_{i,m-1} \\ &= \frac{(\mathbf{1}_{\mathcal{E}_m}^\top (\tilde{X}_{\mathcal{E}_m} \tilde{X}_{\mathcal{E}_m}^\top)^{-1} \tilde{X}_{\mathcal{E}_m} \tilde{x}_i - 1) b_{i,m-1}}{\mathbf{1}_{\mathcal{E}_m}^\top (\tilde{X}_{\mathcal{E}_m} \tilde{X}_{\mathcal{E}_m}^\top)^{-1} \mathbf{1}_{\mathcal{E}_m}} + \tilde{x}_i^\top \tilde{X}_{\mathcal{E}_m}^\top ((\tilde{X}_{\mathcal{E}_m} \tilde{X}_{\mathcal{E}_m}^\top)^{-1} \tilde{X}_{\mathcal{E}_m} \tilde{x}_i b_{i,m-1} - \tilde{x}_i^\top \tilde{x}_i b_{i,m-1} \\ &\quad - \frac{(\tilde{X}_{\mathcal{E}_m} \tilde{X}_{\mathcal{E}_m}^\top)^{-1} \mathbf{1}_{\mathcal{E}_m} (\mathbf{1}_{\mathcal{E}_m}^\top (\tilde{X}_{\mathcal{E}_m} \tilde{X}_{\mathcal{E}_m}^\top)^{-1} \tilde{X}_{\mathcal{E}_m} \tilde{x}_i - 1) b_{i,m-1}}{\mathbf{1}_{\mathcal{E}_m}^\top (\tilde{X}_{\mathcal{E}_m} \tilde{X}_{\mathcal{E}_m}^\top)^{-1} \mathbf{1}_{\mathcal{E}_m}}) \\ &= b_{i,m-1} \left(-\frac{(\mathbf{1}_{\mathcal{E}_m}^\top (\tilde{X}_{\mathcal{E}_m} \tilde{X}_{\mathcal{E}_m}^\top)^{-1} \tilde{X}_{\mathcal{E}_m} \tilde{x}_i - 1)^2}{\mathbf{1}_{\mathcal{E}_m}^\top (\tilde{X}_{\mathcal{E}_m} \tilde{X}_{\mathcal{E}_m}^\top)^{-1} \mathbf{1}_{\mathcal{E}_m}} - \tilde{x}_i^\top (I - \tilde{X}_{\mathcal{E}_m}^\top (\tilde{X}_{\mathcal{E}_m} \tilde{X}_{\mathcal{E}_m}^\top)^{-1} \tilde{X}_{\mathcal{E}_m}) \tilde{x}_i \right).\end{aligned}$$

This proves (40).

Moreover, under the *general position condition*, we must have the rows of $\tilde{X}_{\mathcal{E}_m}$ and \tilde{x}_i are linearly independent since $|\mathcal{E}_m \cup \{i\}| = |\mathcal{E}_{m-1}| \leq \min(n, p+1) \leq \min(n, p+2)$. Hence, $\tilde{x}_i^\top (I - \tilde{X}_{\mathcal{E}_m}^\top (\tilde{X}_{\mathcal{E}_m} \tilde{X}_{\mathcal{E}_m}^\top)^{-1} \tilde{X}_{\mathcal{E}_m}) \tilde{x}_i > 0$ since $\tilde{X}_{\mathcal{E}_m}^\top (\tilde{X}_{\mathcal{E}_m} \tilde{X}_{\mathcal{E}_m}^\top)^{-1} \tilde{X}_{\mathcal{E}_m}$ is the projection matrix for the row space of $\tilde{X}_{\mathcal{E}_m}$ and $\tilde{X}_{\mathcal{E}_m}^\top (\tilde{X}_{\mathcal{E}_m} \tilde{X}_{\mathcal{E}_m}^\top)^{-1} \tilde{X}_{\mathcal{E}_m} \tilde{x}_i \neq \tilde{x}_i$. Thus, in order to show that the LHS of (39) is positive, it remains to show that $b_{i,m-1} < 0$. Based on the facts that $\hat{\theta}_{i,\omega}$ is a linear function of ω : $\hat{\theta}_{i,\omega} = \hat{\theta}_{i,\omega_{m-1}} + b_{i,m-1}(\omega - \omega_{m-1})$ for $\omega \in [\omega_m, \omega_{m-1}]$ and $\hat{\theta}_{i,\omega} = \tau$ at ω_m , we must have its slope $\frac{\partial \hat{\theta}_{i,\omega}}{\partial \omega} < 0$ for $\omega \in (\omega_m, \omega_{m-1})$. This implies that

$$\frac{\partial \hat{\theta}_{i,\omega}}{\partial \omega} = b_{i,m-1} < 0,$$

which completes the proof for rule (a).

For rule (b), similar arguments can be applied to prove that if there exists some case $i \in \mathcal{E}_{m-1}$ such that $\hat{\theta}_{i,\omega_m} = \tau - 1$ and $r_{i,\omega_m} = 0$ at ω_m , then $r_{i,\omega} < 0$ for any $\omega \in (\omega_{m+1}, \omega_m)$.

For rule (c), without loss of generality, we assume that $r_{i,\omega_m} = 0$ for some case $i \in \mathcal{L}_{m-1}$ and $\hat{\theta}_{i,\omega_m} = \tau - 1$ at ω_m . Then the rule updates the three sets as $\mathcal{E}_m = \mathcal{E}_{m-1} \cup \{i\}$ and

$\mathcal{L}_m = \mathcal{L}_{m-1} \setminus \{i\}$. As ω starts to decrease from ω_m , $\hat{\theta}_{i,\omega}$ will increase from $\tau - 1$, which implies that its slope $b_{i,m} < 0$.

In the proof of rule (a), we have shown that $h_{i,m} < 0$ given $b_{i,m-1} < 0$ and $h_{i,m-1} = 0$. Here we need to prove $b_{i,m} < 0$ given $h_{i,m-1} < 0$ and $h_{i,m} = 0$. Reversing the arguments used for rule (a), we need to show that $b_{i,m} < 0$ given (39). Similar to the proof of rule (a), we can show that the LHS of (39) is

$$b_{i,m} \left(-\frac{(\mathbf{1}_{\mathcal{E}_{m-1}}^\top (\tilde{X}_{\mathcal{E}_{m-1}} \tilde{X}_{\mathcal{E}_{m-1}}^\top)^{-1} \tilde{X}_{\mathcal{E}_{m-1}} \tilde{x}_i - 1)^2}{\mathbf{1}_{\mathcal{E}_{m-1}}^\top (\tilde{X}_{\mathcal{E}_{m-1}} \tilde{X}_{\mathcal{E}_{m-1}}^\top)^{-1} \mathbf{1}_{\mathcal{E}_{m-1}}} - \tilde{x}_i^\top (I - \tilde{X}_{\mathcal{E}_{m-1}}^\top (\tilde{X}_{\mathcal{E}_{m-1}} \tilde{X}_{\mathcal{E}_{m-1}}^\top)^{-1} \tilde{X}_{\mathcal{E}_{m-1}}) \tilde{x}_i \right) > 0,$$

which implies that $b_{i,m} < 0$. This completes the proof.

A.6 Proof of Proposition 2

The normal equation for problem (16) is

$$-\sum_{i \neq i^*}^n \tilde{x}_i (y_i - \tilde{x}_i^\top \tilde{\beta}_\omega) - \omega \tilde{x}_{i^*} (y_{i^*} - \tilde{x}_{i^*}^\top \tilde{\beta}_\omega) + \lambda \tilde{I} \tilde{\beta}_\omega = 0. \quad (45)$$

When $\omega = \omega_0 = 1$, in particular, the normal equation is

$$-\sum_{i \neq i^*}^n \tilde{x}_i (y_i - \tilde{x}_i^\top \tilde{\beta}_{\omega_0}) - \omega \tilde{x}_{i^*} (y_{i^*} - \tilde{x}_{i^*}^\top \tilde{\beta}_{\omega_0}) - (1 - \omega) \tilde{x}_{i^*} (y_{i^*} - \tilde{x}_{i^*}^\top \tilde{\beta}_{\omega_0}) + \lambda \tilde{I} \tilde{\beta}_{\omega_0} = 0. \quad (46)$$

Subtracting (45) from (46), we have

$$\left[\sum_{i \neq i^*}^n \tilde{x}_i \tilde{x}_i^\top + \omega \tilde{x}_{i^*} \tilde{x}_{i^*}^\top + \lambda \tilde{I} \right] (\tilde{\beta}_{\omega_0} - \tilde{\beta}_\omega) = (1 - \omega) \tilde{x}_{i^*} (y_{i^*} - \tilde{x}_{i^*}^\top \tilde{\beta}_{\omega_0}) = (1 - \omega) \tilde{x}_{i^*} r_{i^*},$$

which leads to

$$\tilde{\beta}_{\omega_0} - \tilde{\beta}_\omega = [\tilde{X}^\top \tilde{X} + \lambda \tilde{I} - (1 - \omega) \tilde{x}_{i^*} \tilde{x}_{i^*}^\top]^{-1} (1 - \omega) \tilde{x}_{i^*} r_{i^*}.$$

Letting $\tilde{D}_\lambda = \tilde{X}^\top \tilde{X} + \lambda \tilde{I}$, we have

$$\begin{aligned}
\tilde{\beta}_{\omega_0} - \tilde{\beta}_\omega &= \left[\tilde{D}_\lambda^{-1} + \frac{\tilde{D}_\lambda^{-1} \tilde{x}_{i^*} \tilde{x}_{i^*}^\top \tilde{D}_\lambda^{-1}}{1/(1-\omega) - \tilde{x}_{i^*}^\top \tilde{D}_\lambda^{-1} \tilde{x}_{i^*}} \right] (1-\omega) \tilde{x}_{i^*} r_{i^*} \\
&= (1-\omega) \tilde{D}_\lambda^{-1} \left[\tilde{x}_{i^*} + \frac{\tilde{x}_{i^*} \tilde{x}_{i^*}^\top \tilde{D}_\lambda^{-1} \tilde{x}_{i^*}}{1/(1-\omega) - \tilde{x}_{i^*}^\top \tilde{D}_\lambda^{-1} \tilde{x}_{i^*}} \right] r_{i^*} \\
&= \frac{\tilde{D}_\lambda^{-1} \tilde{x}_{i^*} r_{i^*}}{1/(1-\omega) - \tilde{x}_{i^*}^\top \tilde{D}_\lambda^{-1} \tilde{x}_{i^*}},
\end{aligned}$$

which implies that

$$\hat{f}(x_j) - \hat{f}_\omega^{i^*}(x_j) = \tilde{x}_j^\top (\tilde{\beta}_{\omega_0} - \tilde{\beta}_\omega) = \frac{(\tilde{x}_j^\top \tilde{D}_\lambda^{-1} \tilde{x}_{i^*}) r_{i^*}}{1/(1-\omega) - \tilde{x}_{i^*}^\top \tilde{D}_\lambda^{-1} \tilde{x}_{i^*}} = \frac{h_{ji^*}(\lambda) r_{i^*}}{1/(1-\omega) - h_{i^*i^*}(\lambda)}. \quad (47)$$

Hence,

$$\sum_{j=1}^n (\hat{f}(x_j) - \hat{f}_\omega^{i^*}(x_j))^2 = \frac{r_{i^*}^2 \sum_{j=1}^n h_{ji^*}^2(\lambda)}{\{1/(1-\omega) - h_{i^*i^*}(\lambda)\}^2},$$

which completes the proof.

Table 1: Approximation Error of $\rho_\tau(r_i^{[-i]}) - \rho_\tau(r_i)$

Scenario		True Difference	Approximation	Approximation Error
$r_i^{[-i]}$	r_i	$\rho_\tau(r_i^{[-i]}) - \rho_\tau(r_i)$	$\rho'_{\tau,\delta}(r_i)(r_i^{[-i]} - r_i)$	$\Delta_{\text{approx.}}$
(a)	$(0, \infty) \quad (-\infty, -\delta]$	$(\tau) r_i^{[-i]} - (\tau - 1) r_i$	$(\tau - 1)(r_i^{[-i]} - r_i)$	$- r_i^{[-i]} $
(b)	$(0, \infty) \quad (-\delta, 0]$		$2(1 - \tau) \frac{r_i}{\delta} (r_i^{[-i]} - r_i)$	$\approx -\tau r_i^{[-i]} $
(c)	$(-\infty, 0) \quad [\delta, \infty)$	$(\tau - 1) r_i^{[-i]} - (\tau) r_i$	$\tau (r_i^{[-i]} - r_i)$	$- r_i^{[-i]} $
(d)	$(-\infty, 0) \quad [0, \delta)$		$2\tau \frac{r_i}{\delta} (r_i^{[-i]} - r_i)$	$\approx -(1 - \tau) r_i^{[-i]} $

A.7 Data Analysis

A.7.1 King County House Sales Data

Luan et al. (2022) considered the King County House Sales Data for hetero-scedastic linear regression. Based on the exploratory data analysis results, 12 features were selected, and

Table 2: Average number of ω -breakpoints for various data dimensions and quantiles. The results are averaged over 20 independent simulations with $N_\lambda = 50$. The 50 grid points for $\lambda \in [0.01, 100]$ are equally spaced on the logarithmic scale. The values in the parentheses are the corresponding standard errors.

τ	n	p	Average number of ω breakpoints	n	p	Average number of ω breakpoints
0.1	100	50	4.409 (0.556)	50	300	0.714 (0.109)
	300	50	4.417 (0.768)	150	300	1.044 (0.192)
0.3	100	50	7.177 (0.686)	50	300	0.714 (0.109)
	300	50	7.724 (1.074)	150	300	1.360 (0.202)
0.5	100	50	7.427 (0.695)	50	300	1.098 (0.119)
	300	50	8.780 (1.119)	150	300	1.635 (0.238)

Table 3: The elapsed runtime per case (i.e., the total runtime/ n) measured in seconds for LOO CV simulation ($p = 50$ and $n > p$). The value in the parentheses is the standard deviation over 20 replicates.

n	p	τ	λ -path ($N_\lambda = 50$)	w -path ($N_\lambda = 20$)	w -path ($N_\lambda = 50$)
100	50	0.1	0.0025 (0.0003)	0.0027 (0.0005)	0.0065 (0.0010)
100	50	0.3	0.0040 (0.0006)	0.0045 (0.0005)	0.0110 (0.0013)
100	50	0.5	0.0047 (0.0005)	0.0051 (0.0008)	0.0127 (0.0020)
200	50	0.1	0.0091 (0.0013)	0.0036 (0.0006)	0.0089 (0.0014)
200	50	0.3	0.0238 (0.0034)	0.0089 (0.0014)	0.0222 (0.0035)
200	50	0.5	0.0309 (0.0053)	0.0101 (0.0013)	0.0251 (0.0032)
300	50	0.1	0.0216 (0.0030)	0.0050 (0.0008)	0.0124 (0.0019)
300	50	0.3	0.0699 (0.0061)	0.0117 (0.0014)	0.0294 (0.0033)
300	50	0.5	0.0904 (0.0124)	0.0138 (0.0019)	0.0344 (0.0049)

appropriate transformations were applied to the selected features. In this paper, we utilize the same features for an l_2 -penalized quantile regression. Table 5 lists all 12 variables, and details of the data transformations can be found in Appendix B.2 of Luan et al. (2022).

A.7.2 Exploratory Data Analysis (EDA)

We present EDA results for the random sample of 200 houses. Based on the plots in Figure 14, we dropped some features with insufficient variability to prevent unreliable estimates. For example, the waterfront feature was excluded because only 1 out of 200

Table 4: The runtime per case for LOO CV simulation ($p = 300$ and $n < p$). The value in the parentheses is the standard deviation over 20 replicates.

n	p	τ	λ -path ($N_\lambda = 50$)	w -path ($N_\lambda = 20$)	w -path ($N_\lambda = 50$)
50	300	0.1	0.0018 (2e-5)	0.0015 (3e-5)	0.0036 (9e-5)
50	300	0.3	0.0018 (5e-5)	0.0016 (3e-5)	0.0038 (6e-5)
50	300	0.5	0.0018 (2e-5)	0.0016 (4e-5)	0.0039 (6e-5)
100	300	0.1	0.0098 (7e-5)	0.0039 (0.00014)	0.0097 (0.00018)
100	300	0.3	0.0098 (8e-5)	0.0043 (0.00011)	0.0107 (0.00020)
100	300	0.5	0.0099 (1e-4)	0.0045 (0.00017)	0.0111 (0.00022)
150	300	0.1	0.0254 (0.00020)	0.0074 (0.00031)	0.0182 (0.00050)
150	300	0.3	0.0260 (0.00040)	0.0081 (0.00033)	0.0203 (0.00049)
150	300	0.5	0.0260 (0.00035)	0.0084 (0.00031)	0.0208 (0.00047)

Table 5: List of independent variables used in King County house sales data analysis

Variable	Type	Description	Transformation
basement	categorical	Whether the house has basement or not: yes/no	-
bathrooms	numeric	Number of bathrooms in the house	-
bedrooms	categorical	Number of bedrooms in the house: 1-2/3-5/6 or more	-
condition	categorical	Condition of the house: poor/average/good	-
grade	numeric	Overall grade of the house regarding the types of materials used and the quality of workmanship	-
grade2	numeric	Square of grade	-
sqft_living	numeric	Interior living space of the houses in square feet	square root
sqft_living15	numeric	Average interior living space for the closest 15 houses in square feet	square root
view	numeric	Grade of the view around the house	-
waterfront	categorical	Whether the house has a waterfront or not: yes/no	-
yr_built	categorical	Year when the house was built: 1920 or before/1921-1940/1941-1960/1961-1980/1981-2000/2001 or after	-
zone	categorical	Location of the house: zone 1/zone 2/zone 3	-

houses overlooked the waterfront. Similarly, the zone feature was dropped due to low variability. Since there are no houses in poor condition in our sample, we used average condition as the baseline. Since there are only 2 houses with more than 6 bedrooms, we decided to combine this category with the 3-5 bedrooms category. For the view of the house, since most houses have a score of 0, we decided to combine the non-zero scores into one category and treat it as a categorical variable.

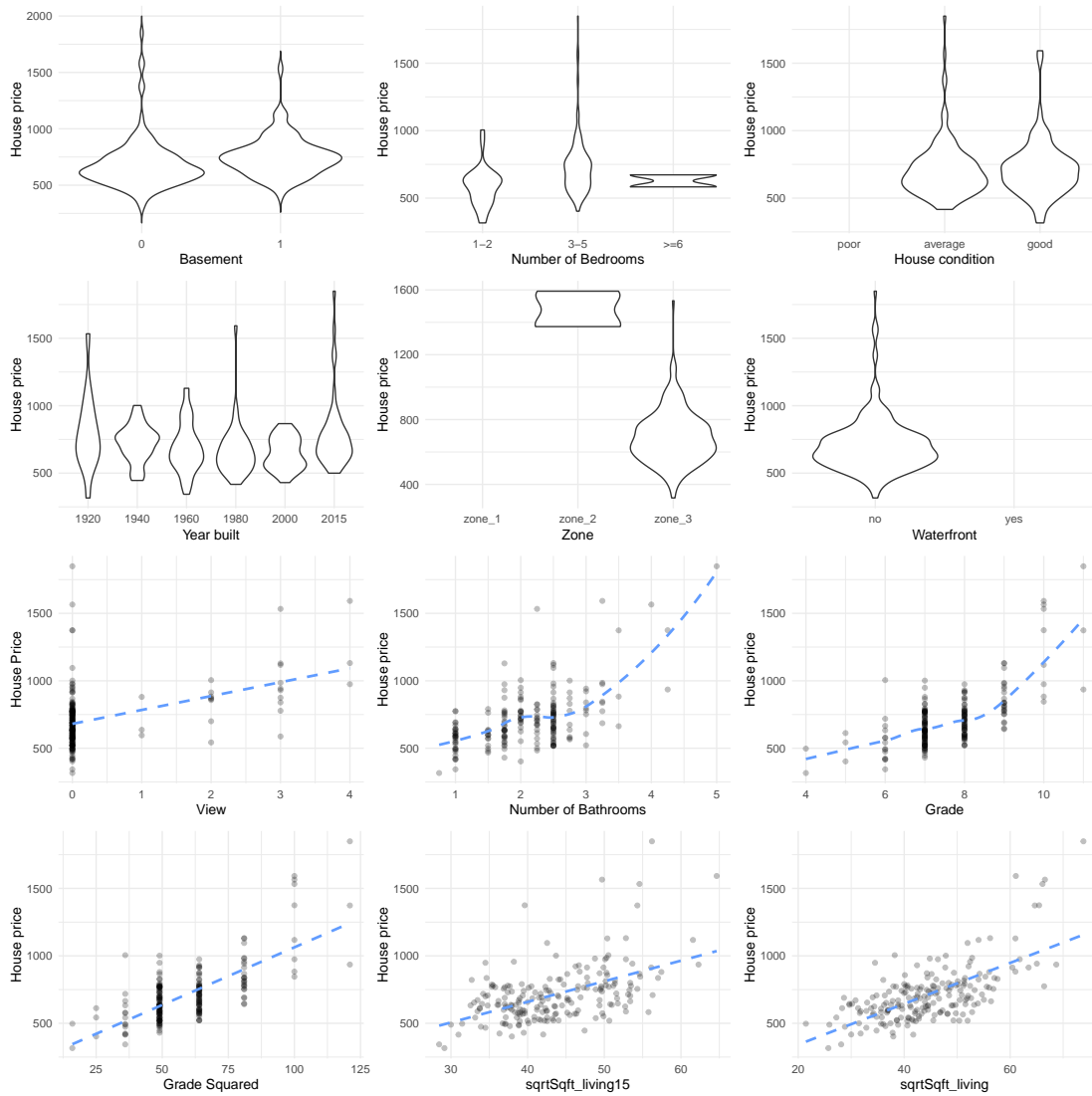


Figure 14: EDA plots for a random sample of 200 houses with the view of the house treated as a numeric variable.

A.7.3 Proof of the Piece-wise Constant Pattern in Case-Influence Graph

Proposition 4. *For linear quantile regression, if the elbow set at ω_m is of full rank, i.e., $|\mathcal{E}_m| = p + 1$, the solution path $\hat{f}_\omega(x)$ is constant for $\omega \in (\omega_{m+1}, \omega_m]$.*

Proof. From Equation (21) for $m = 0$, we can conclude that when the initial elbow set is of full rank, i.e. $|\mathcal{E}_0| = p + 1$, the solution path between two consecutive breakpoints ω_1 and $\omega_0 = 1$ is constant. When $|\mathcal{E}_0| = p + 1$, the projection matrix onto the space spanned by the elbow set points $P_{\tilde{X}_{\mathcal{E}_0}}$ is I , which makes the second part of the following term zero:

$$\left[\frac{(q_0^\top \tilde{x}_i - 1)(q_0^\top \tilde{x}_{i^*} - 1)}{q_0^\top q_0} + \tilde{x}_i^\top (I - P_{\tilde{X}_{\mathcal{E}_0}}) \tilde{x}_{i^*} \right].$$

In addition, since \tilde{x}_{i^*} is in the row space of $\tilde{X}_{\mathcal{E}_0}$, there exists $a \in \mathbb{R}^{p+1}$ such that $\tilde{x}_{i^*} = \tilde{X}_{\mathcal{E}_0}^\top a$, which also implies $1_{p+1}^\top a = 1$. In this case, the first part of the term also becomes zero because

$$(q_0^\top \tilde{x}_{i^*} - 1) = 1_{\mathcal{E}_0}^\top \left(\tilde{X}_{\mathcal{E}_0} \tilde{X}_{\mathcal{E}_0}^\top \right)^{-1} \tilde{X}_{\mathcal{E}_0} (\tilde{X}_{\mathcal{E}_0}^\top a) - 1 = 1_{p+1}^\top a - 1 = 0.$$

This conclusion for the solution path at $\omega_0 = 1$ holds true generally for any breakpoints ω_m , as long as the elbow set at ω_m is of full rank since the rate of change of the case-weight adjusted solution at $\omega \in (\omega_{m+1}, \omega_m]$ is

$$\frac{\partial \hat{f}_\omega(x_i)}{\partial \omega} = \frac{1}{\lambda} \left[\frac{(q_m^\top \tilde{x}_i - 1)(q_m^\top \tilde{x}_{i^*} - 1)}{q_m^\top q_m} + \tilde{x}_i^\top (I - P_{\tilde{X}_{\mathcal{E}_m}}) \tilde{x}_{i^*} \right] \cdot (\tau - \mathbb{I}(i^* \in \mathcal{L}_m)), \quad (48)$$

where $q_m = \tilde{X}_{\mathcal{E}_m}^\top \left(\tilde{X}_{\mathcal{E}_m} \tilde{X}_{\mathcal{E}_m}^\top \right)^{-1} 1_{\mathcal{E}_m} \in \mathbb{R}^{p+1}$. □

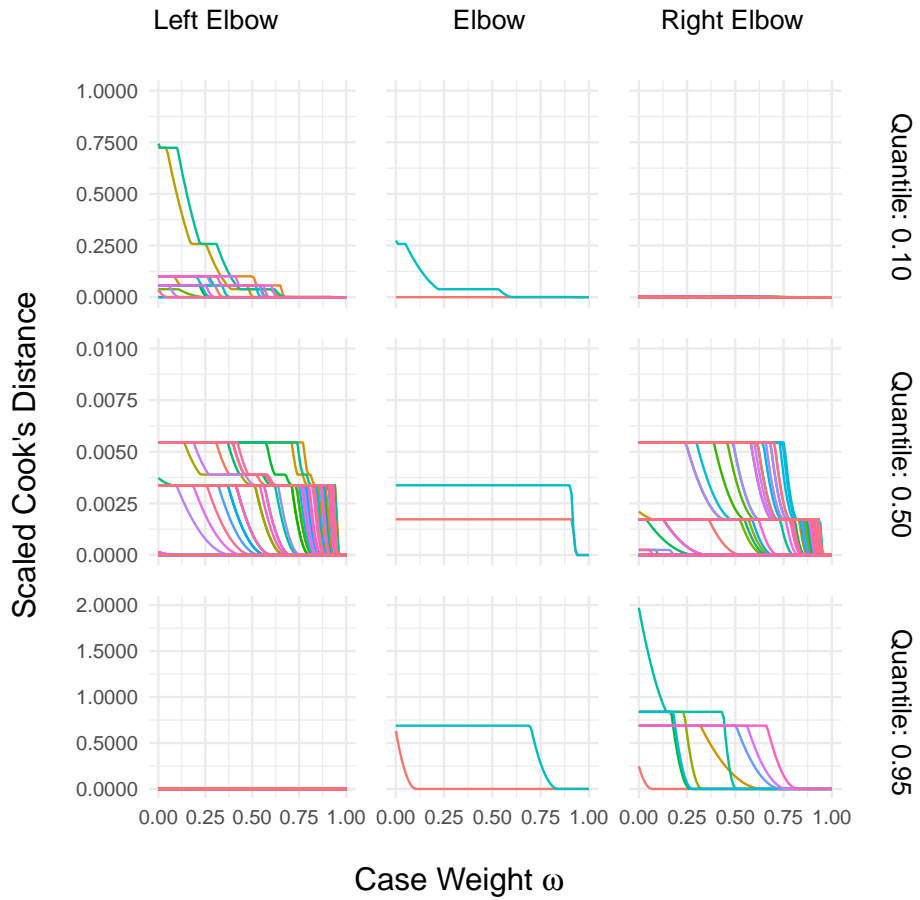


Figure 15: Case-influence graphs from the single-predictor quantile regression for the King County house sales data with various quantiles: $\tau = 0.1$ (top), 0.5 (middle) and 0.95 (bottom). The left, middle and right panels correspond to the left elbow, elbow and right elbow set points, respectively.

A.7.4 LOO Solutions for Quantile Regression with Multiple Predictors

We present a comprehensive comparison of the full-data solution and the LOO solution excluding the observation with the largest Cook’s distance for each quantile. In Tables 6, 7 and 8, the first column lists the feature names after the corresponding transformations described in Table 5. The second column contains the estimated coefficients based on the random sample of 200 observations (full-data solution), and their corresponding p-values. The third column provides the estimated coefficients when excluding the observation with the largest Cook’s distance (LOO solution) and corresponding p-values. The calculation is based on the standard quantile regression function in the R package `quantreg` (Koenker et al., 2018) with no regularization applied.

Those features whose statistical significance may change between the full-data and LOO solutions (using the significance level of 0.05) are highlighted in bold in the first column. Among the three tables, at $\tau = 0.5$, we observe no noticeable changes in the p-values even when excluding the most influential observation, demonstrating the robustness of median regression. In contrast, at $\tau = 0.95$, statistical significance of multiple features is affected by the most influential observation.

Table 6: Estimated quantile regression coefficients and their p-values when $\tau = 0.1$.

Feature	Full-Data Solution	LOO Solution
basement	28.79 (0.30)	28.61 (0.28)
bathrooms	63.27 (0.01)	63.29 (0.02)
condition_good	-18.81 (0.46)	-18.94 (0.46)
yr_built_2000	-29.92 (0.34)	-30.06 (0.32)
yr_built_1980	40.01 (0.26)	39.28 (0.29)
yr_built_1960	75.98 (0.04)	75.71 (0.06)
yr_built_1940	129.21 (0.03)	128.93 (0.04)
yr_built_1920	185.44 (0.00)	184.41 (0.00)
grade	48.72 (0.54)	47.90 (0.55)
grade2	1.31 (0.80)	1.35 (0.80)
sqrtSqft_living15	1.00 (0.67)	0.95 (0.74)
sqrtSqft_living	-0.76 (0.67)	-0.71 (0.74)
bedrooms_3	56.69 (0.30)	56.72 (0.28)
view	107.93 (0.00)	109.32 (0.00)

Table 7: Estimated quantile regression coefficients and their p-values when $\tau = 0.5$.

Feature	Full-Data Solution	LOO Solution
basement	16.61 (0.57)	14.06 (0.67)
bathrooms	28.13 (0.21)	26.78 (0.23)
condition_good	34.40 (0.17)	34.58 (0.15)
yr_built_2000	-32.01 (0.33)	-32.17 (0.35)
yr_built_1980	25.43 (0.48)	27.03 (0.52)
yr_built_1960	88.03 (0.03)	89.33 (0.03)
yr_built_1940	160.14 (0.00)	161.38 (0.00)
yr_built_1920	143.66 (0.00)	146.13 (0.01)
grade	-62.22 (0.69)	-83.10 (0.56)
grade2	10.48 (0.31)	11.92 (0.22)
sqrtSqft_living15	1.76 (0.49)	1.61 (0.51)
sqrtSqft_living	4.11 (0.18)	4.45 (0.15)
bedrooms_3	-30.28 (0.39)	-28.98 (0.35)
view	30.08 (0.51)	24.82 (0.55)

Table 8: Estimated quantile regression coefficients and their p-values when $\tau = 0.95$.

Feature	Full-data Solution	LOO Solution
basement	-58.00 (0.18)	-53.70 (0.21)
bathrooms	104.03 (0.02)	77.47 (0.05)
condition_good	23.15 (0.53)	18.67 (0.58)
yr_built_2000	-63.32 (0.41)	-105.47 (0.10)
yr_built_1980	-8.16 (0.91)	-68.91 (0.32)
yr_built_1960	63.44 (0.53)	21.55 (0.83)
yr_built_1940	113.47 (0.13)	41.39 (0.62)
yr_built_1920	78.20 (0.41)	91.33 (0.38)
grade	-523.42 (0.05)	-370.92 (0.12)
grade2	40.36 (0.02)	29.02 (0.06)
sqrtSqft_living15	-0.27 (0.96)	-2.85 (0.57)
sqrtSqft_living	4.95 (0.23)	8.10 (0.04)
bedrooms_3	-55.37 (0.34)	-25.40 (0.64)
view	121.15 (0.17)	137.01 (0.05)